Available online at www.sciencedirect.com
ScienceDirect
Lithos 91 (2006) 262–285
LITHOS
www.elsevier.com/locate/lithos

Influence of oxygen fugacity on mineral compositions in peralkaline melts: The Katzenbuckel volcano, Southwest Germany

Ute Mann, Michael Marks, Gregor Markl *

Institut für Geowissenschaften, AB Mineralogie und Geodynamik, Eberhard-Karls-Universität, Wilhelmstrasse 56, D-72074 Tübingen, Germany

Received 18 October 2004; accepted 5 September 2005
Available online 28 November 2005

Abstract

The igneous rocks of the Katzenbuckel, Southwest Germany, represent a unique and unusual alkaline to peralkaline association within the European Volcanic Province. The magmatic activity can be subdivided into two main phases. Phase I comprises the main rock bodies of phonolite and nepheline syenite, which were later intruded by different peralkaline dyke rocks (tinguaites and alkali feldspar syenite dykes) of phase II. The dyke assemblage was accompanied by magnetite and apatite veins and was followed by a late-stage pneumatolytic activity causing autometasomatic alterations.

As is typical for alkaline to peralkaline igneous rocks, early mafic minerals of phase I rocks comprise olivine, augite and Fe–Ti oxides, which are substituted in the course of fractionation by Na-amphibole and Na-pyroxene. For the early magmatic stage, calculated temperatures range between 880 and 780 °C with low silica activities (0.4 to 0.6) but high relative oxygen fugacities between 0.5 and 1.9 log units above the FMQ buffer. Even higher oxygen fugacities (above the HM buffer) are indicated for the autometasomatic alteration, which occurred at temperatures between 585 and 780 °C and resulted in the formation of pseudobrookite and hematite.

The unusually high oxygen fugacities (even during the early magmatic stage) are recorded by the major element compositions of the mafic minerals (forsterite content in olivine between 68 and 78 mol%, up to 6.2 wt.% ZrO_2 and 8.5 wt.% TiO_2 in clinopyroxene), the unusual mineral assemblages (pseudobrookite, freudenbergite) and by the enrichment of Fe^{3+} in the felsic minerals (up to 2.8 wt.% Fe_2O_3 in alkali feldspar and up to 2.6 wt.% Fe_2O_3 in nepheline). These observations point to a metasomatically enriched and highly oxidized lithospheric mantle as a major source for the Katzenbuckel melts.

Keywords: Peralkaline; Oxygen fugacity; Ti–Zr-rich aegirine; Pseudobrookite; Metasomatism

1. Introduction

Alkaline and peralkaline igneous rocks represent a volumetrically small but highly variable group of igneous rocks typically located within intracontinental extensional environments (Wilson, 1989). Generally, they are characterized by high contents of alkalis, halogens and rare and incompatible elements such as e.g., Li, Rb, Zr, Zn, Nb and REE and low concentrations of compatible elements like Mg, Ca, Cr, Co and Ni (Sørensen, 1997).

These chemical characteristics result in an unusual mineral assemblage: otherwise scarce minerals can appear as rock-forming phases (e.g., aegirine, arfvedsonite) and are accompanied by a variety of rare accessory minerals among which Na–Ti–Nb-oxides (e.g. pyrochlore) Na–Ti-silicates (e.g. lorenzenite) or Na–Zr-silicates (e.g. eudialyte) predominate.

* Corresponding author. Tel.: +49 7071 2972930.
E-mail address: markl@uni-tuebingen.de (G. Markl).

0024-4937/$ - see front matter © 2005 Elsevier B.V. All rights reserved.
doi:10.1016/j.lithos.2005.09.004

Various experimental (e.g., Sood and Edgar, 1970; Edgar and Parker, 1974; Kogarko and Romanchev, 1977) and field studies (e.g., Larsen and Sørensen, 1987; Markl et al., 2001; Marks and Markl, 2001; Marks et al., 2003) showed that water pressure and oxygen fugacity are critical factors that influence the formation and the chemical evolution of peralkaline melts. Solidus temperatures of some agpaitic melts may be as low as 400 °C. As low initial water contents and/or low oxygen fugacity prevent the early exsolution of a fluid phase (Kogarko, 1977; Khomyakov, 1995) alkalis and volatiles are therefore retained in the melt and finally enriched in the hydrothermal fluid separated from the low-temperature melt in the very late-magmatic stage (Sørensen, 1997). These residual fluids give rise to a number of mineralizations documented in the exotic assemblages of pegmatites and hydrothermal veins (e.g., Salvi and Williams-Jones, 1990; Chakhmouradian and Mitchell, 2002; Markl et al., 2001; Markl and Baumgartner, 2002; Marks et al., 2003). Other important effects are metasomatic alterations (fenitization) that mainly affect the exocontact zone of an intrusion (e.g. Morogan, 1989).

The alkaline rocks of the Katzenbuckel, Southwest Germany, which are the topic of the present study, comprise a small occurrence of silica-undersaturated and peralkaline sodic rocks (phase I), which were intruded by various peralkaline dykes (phase II). During the late-magmatic stage, phase I rocks were subject to metasomatic overprinting in some places. This event was accompanied by hydrothermal magnetite and apatite mineralizations. In the present contribution we focus on the mineral chemistry and the petrology of the main rock types. The data are used to discuss the influence of intrinsic parameters such as oxygen fugacity on the observed compositional trends in the rock-forming minerals. We compare them to similar rock types worldwide and finally try to deduce geochemical constraints on the magma source region for the Katzenbuckel rocks.

2. Regional geology

2.1. The Cenozoic alkaline magmatism of western and central Europe

The Katzenbuckel volcano belongs to a group of Cenozoic alkaline intracontinental volcanic complexes in western and central Europe that are concentrated in three provinces, which are mainly situated within Variscan massifs (Fig. 1a). Their centres lie in the Massif Central, the Bohemian Massif and in the

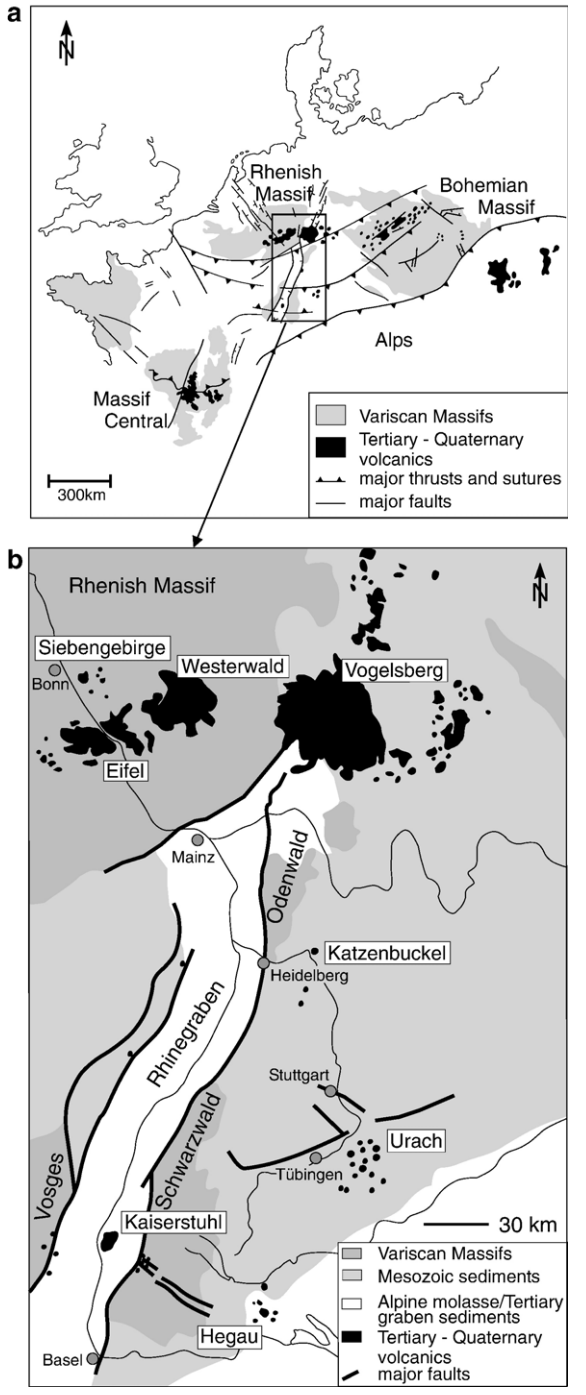

Fig. 1. (a) Schematic map of the western and central European Cenozoic volcanic provinces and their location within the Variscan massifs (modified after Wilson and Downes, 1991). (b) Map of the German Cenozoic volcanic province with some of the more important occurrences of volcanic rocks of the Rhenish Massif, the Vogelsberg and the Rhinegraben area indicated.

Rhenish Massif (e.g., Eifel, Westerwald, Siebengebirge) including the Vogelsberg volcanic complex and its neighboring areas to the north and east (Fig. 1b). A number of smaller occurrences (Kaiserstuhl, Urach, Hegau) are found within and in the surroundings of the Tertiary Rhinegraben. The Katzenbuckel is located in the southeastern part of the Odenwald (Southwest Germany) about 25 km east of the Rhinegraben (Fig. 1b).

Volcanic activity in the three European regions lasted for a period of more than 60 Ma, starting in the Upper Cretaceous and reaching its climax in the Miocene, continuing to the Quaternary only in few regions with the youngest (10 kA) in the Laacher See area (Eifel). K/Ar-ages of 65 Ma (biotite) and 55 Ma (whole rock) place the Katzenbuckel rocks among the oldest of this group (Lippolt et al., 1963, 1976).

The magmatism in all three provinces is dominated by sodic primitive magmas ranging from melilitites, melilite nephelinites and olivine nephelinites through basanites to alkali olivine basalts (Wilson and Patterson, 2001). Differentiates of these rocks are subordinate and typically appear in bimodal assemblages (e.g. phonolites from Hegau). In few areas, potassic basic magmas such as leucite nephelinites and leucitites can be found (East Eifel, Massif Central).

Based on geochemical and isotopic investigations, Wilson and Downes (1991) and Wedepohl and Baumann (1999) derived models for the genesis and the source regions of the primitive basic magmas. According to these authors, they can be regarded as the product of mixing of partial melts from both asthenospheric and lithospheric mantle sources where the primitive potassic magmas indicate an increasing involvement of an enriched lithospheric component. The spectrum of primitive sodic magmas is considered to represent variable degrees of partial melting of an asthenospheric reservoir that shows the character of a residual depleted mantle (MORB character) mixed with HIMU-like enriched mantle material. The latter is thought to have originated from lithospheric material subducted during the Variscan orogeny.

Table 1
Mineral assemblage of the investigated samples from the Katzenbuckel

	Rock type	Phenocrysts (p), early magmatic minerals	Groundmass minerals, late magmatic minerals	Late-stage hydrothermal minerals, metasomatic minerals	Sample #
Phase I: main intrusive phase	Phonolite	Cpx (p), ± ne (p), ol, ap, mag, ilm, sdl	Ne, bt, aeg, alkfsp,	Zeolites, hem, pseudobrookite, titanian andradite, carbonates	Kb3, KbU2, Kb48, Kb49
	Nepheline syenite	Ne (p), ± cpx (p), ol, ap, mag, ilm, sdl	± Ne, bt, amph, aeg, alkfsp	Amph, aeg, ± Fe-sulfides, zeolites, ± chl, ± hem,	Kb22, Kb24, Kb25, KbU6
Phase II: late-magmatic phase; intrusion of various dyke rocks and hydrothermal veins; metasomatic alteration	Nepheline syenite dykes (tinguaites)	Ne (p), bt, ap, foid minerals, mag, ilm	Alkfsp, aeg	Zeolites, anl, Nb–Ti–Fe oxides, chl, carbonates, Zr oxide	Kb31
		Alkfsp, foid minerals, ± amph, ± aeg	Aeg	± Nb-ilm, ± mag, ± py, ± sp, ± ap, Nb-Zr-Ti oxides, zeolites, aeg, ± Zr-silicates, ± mnz	KbU5, KbU6
	"Normal" alkali feldspar syenite dykes	Alkfsp, foid minerals, amph, aeg	Aeg	Mag, hem, mnz, freudenbergite, pyrochlore, lorenzenite	Kb50
		Alkfsp, foid minerals, cpx, ap, mag, ilm	Bt, ± amph	Zeolites, ± Ti-Nb-(Fe) oxides	KbU4dyke1 Kb47dyke1
		Alkfsp, foid minerals, aeg, amph, mag, ilm, ± ap	± Amph, aeg, ± alkfsp	Aeg, zeolites, ± ap, ± chl, ± Fe-sulfides, ± carbonates	KbU4dyke2 Kb47dyke2
	Alkali feldspar syenite dykes associated with magnetite veins	Alkfsp, amph, ± foid minerals, mag	Amph, aeg	± Aeg, zeolites, ap, Nb-ilm, ± hem, ± zrn, ± pyrochlore, ± carbonates	Kb48, Kb49
	Magnetite veins	Mag, ± mnz, ± ap, carbonates, cpx			Kb48, Kb49

Mineral abbreviations are after Kretz (1983), except for aeg = aegirine.

The tectonomagmatic background of the Cenozoic European volcanism is still not fully understood. However, there is a general consensus that it is intimately related to the alpine extensional tectonics that caused the evolution of Miocene rift-systems in the areas north and west of the alpine fold belt (Wilson and Downes, 1991). On the other hand, gravity (Sobolev et al., 1997) and heat flow measurements (Ritter et al., 2001) indicate thermal anomalies beneath some of the volcanic centres. Based on broadband seismic mantle tomography, several small mantle plumes were proposed for the volcanic fields of the Eifel (Sobolev et al., 1997; Ritter et al., 2001) and the Massif Central (Granet et al., 1995) and it is assumed that their roots reach down to the transition zone.

2.2. The Katzenbuckel volcano

Within the German Rhinegraben province, the Katzenbuckel forms an isolated vent filling with a diameter of about 1 km. It is assumed that a mafic, strongly alkaline melt intruded into a depth of about 600 m below the present surface (Frenzel, 1975). Exsolution of volatiles led to an explosive eruption, leaving behind a cylinder-shaped diatreme. Tuffaceous material with inclusions of fragments from the overlying Mesozoic sediments (e.g. Jurassic limestones and fossils) is interpreted as a fallback breccia that sealed the base of the diatreme (Frenzel, 1975).

At depth, a so-called "sanidine nephelinite" (Rosenbusch, 1869; Table 1) crystallized from the cooling melt. It represents the main rock type of the Katzenbuckel assemblage and makes up more than 90% of the vent filling. Shortly after, a second magma pulse intruded and formed a rock body of about 100 m in diameter. With respect to its mineralogical and chemical composition it strongly resembles the "sanidine nephelinite". Slower cooling rates and the retention of volatiles caused the more plutonic texture of this rock type, which has been termed "Na-shonkinite" (Rosenbusch, 1869). Both rock types are believed to belong to the same magmatic event, which is referred to as the main intrusive phase (phase I, Table 1) in this work. Following the IUGS nomenclature classification scheme (Le Maitre, 2002) the nephelinite (sensu *Rosenbusch*) will be named phonolite and the Na-shonkinite (sensu *Rosenbusch*) as nepheline syenite throughout this study. The second magmatic phase (phase II, Table 1) is characterized by the intrusion of a variety of peralkaline dyke rocks. This dyke assemblage is accompanied by Fe–P–S-mineralizations and the formation of lenses of sulfide minerals. Late-stage pneumatolytic activity caused metasomatic mineralizations and alterations, which are most intense in the outer contact zone of the nepheline syenite body.

3. Petrography

3.1. Research history and investigated sample material

As the Katzenbuckel hill is largely cultivated, natural outcrops of the magmatic rocks are rare. Thus, field relations are mainly based on the early works of Rosenbusch (1869), Lattermann (1887), Freudenberg (1906) and Frenzel (1953, 1961, 1967, 1975). Recent investigations by Stähle et al. (2002) and Stähle and Koch (2003) focused on the rare accessory minerals in the Katzenbuckel rocks. The samples of the present study (Table 1) were taken from the collections of the Mineralogical Institutes of the Universities of Heidelberg and Tübingen.

3.2. Phase I — main intrusive phase

3.2.1. Phonolites (samples KbU2, Kb3, Kb48, Kb49)

This dark grey rock usually has a porphyritic texture. Clinopyroxene phenocrysts show a poikilitic structure (Fig. 2a) with inclusions of magnetite and apatite. Occasionally, their rims are resorbed and overgrown by a later clinopyroxene generation. Microphenocrysts are apatite, a strongly altered sodalite group mineral, olivine, Ti-rich magnetite and ilmenite. The latter three phases are often overgrown by biotite (Fig. 2b). Groundmass minerals are euhedral pyroxene (average grain size 40 μm) and minor amounts of euhedral nepheline (<25 μm). All phases are embedded in anhedral alkali feldspar.

3.2.2. Nepheline syenites (samples Kb22, Kb24, Kb25, KbU6)

This rock type is considered as the plutonic equivalent of the phonolites. Like the latter, it consists of clinopyroxene, olivine, Ti-rich magnetite, ilmenite, apatite, biotite, nepheline, a strongly altered sodalite group mineral, alkali feldspar and amphibole. However, the nepheline syenites show a great variability with respect to modal proportions and texture. A coarse and equigranular grained type (KbU6) can be distinguished from porphyritic types with either nepheline (Kb25) or with both nepheline and clinopyroxene (Kb22, Kb24) as phenocryst phases and some melanocratic varieties also occur. In all samples except Kb25, poikilitic crystals of clinopyroxene and euhedral nepheline (up to 1 cm) can be found. Along cracks, the colour of the clinopyroxene grains becomes more intense (Fig. 2c).

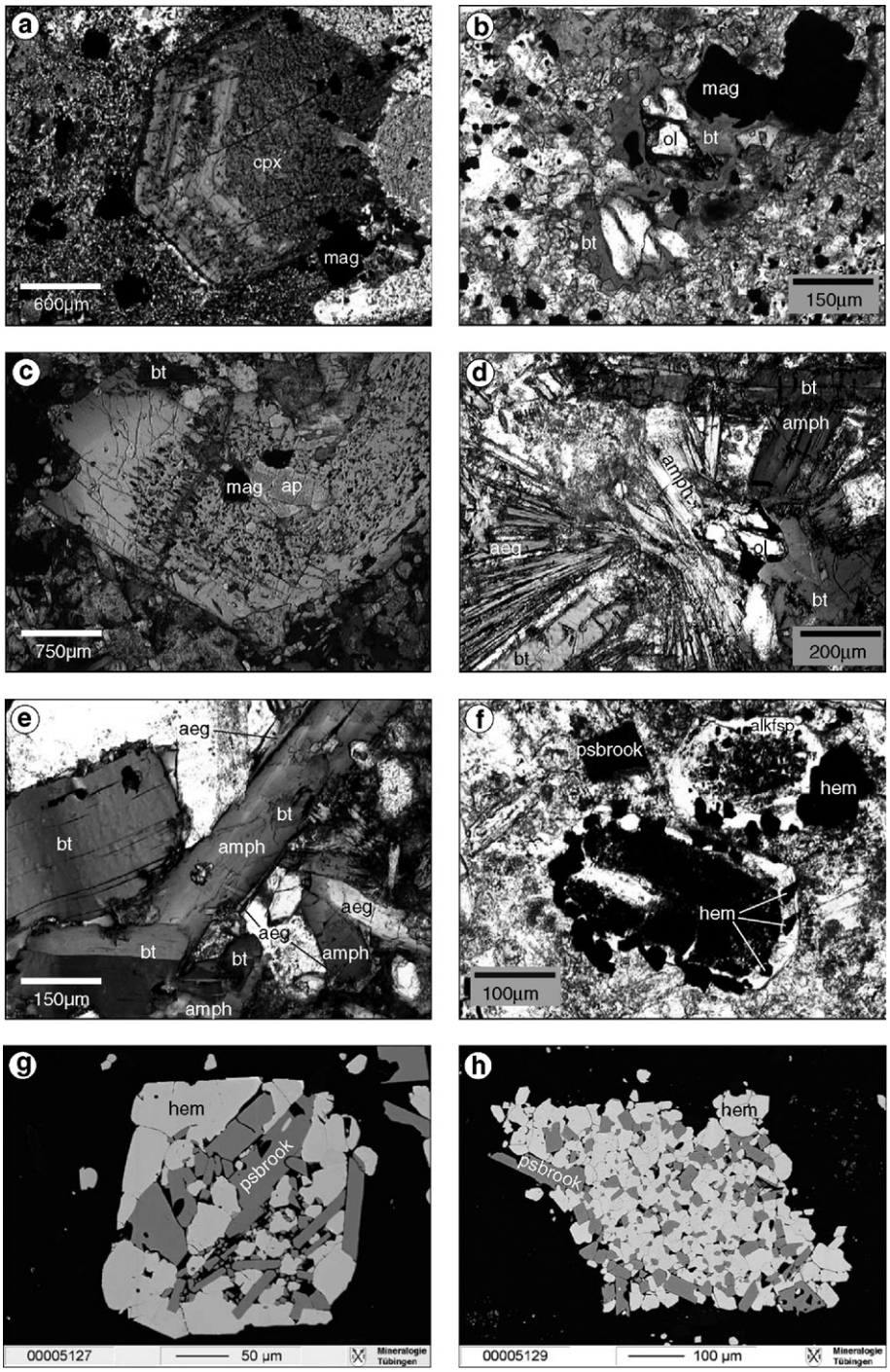

Fig. 2. Petrographic features of phase I rocks from the Katzenbuckel. (a) Zoned poikilitic clinopyroxene phenocryst with many inclusions of magnetite in phonolite Kb3. (b) Magnetite and olivine overgrown by biotite in the same sample. In the groundmass, Fe–Ti oxides and tiny euhedral clinopyroxenes predominate. (c) Large poikilitic clinopyroxene crystal with inclusions of magnetite and apatite from the nepheline syenite KbU6 showing a darker colour towards the margin and along fissures. (d) Radially arranged needles of interstitial aegirine and amphibole partly intergrown with biotite on olivine in nepheline syenite Kb25. (e) Assemblage of biotite, amphibole and aegirine in the nepheline syenite KbU6. (f) Two pseudomorphs of very fine-grained hematite in the centre rimmed by alkali feldspar, possibly replacing olivine in the metasomatically altered phonolite KbU2. (g) and (h) BSE images of aggregates of hematite and pseudobrookite replacing magnetite in the metasomatically altered phonolite KbU2. Mineral abbreviations are after Kretz (1983) except aeg = aegirine and psbrook = pseudobrookite.

In two samples (Kb22, Kb24), a second nepheline generation is present as small (50–100 μm) euhedral grains. Olivine occurs as inclusions within nepheline phenocrysts or alkali feldspar. Magnetite and ilmenite occur as separate phases in variable modal proportions. Biotite, amphibole, aegirine and alkali feldspar are late mineral phases (Fig. 2d and e). Biotite usually forms first among these phases and in two samples (Kb25 and KbU6) it occurs as large euhedral sector-zoned grains up to 2.5 mm. In samples Kb22 and Kb24, anhedral biotite is partly overgrown by amphibole. The intergrowth of amphibole and aegirine indicates their simultaneous crystallization (Fig. 2e).

3.3. Phase II — late magmatic phase

Based on modal and textural criteria, the late magmatic dyke rocks are divided into two main groups. One group includes a number of veins and dykes with a characteristic bluish to greyish green colour, an extremely fine-grained groundmass and a thickness between 0.5 mm and 10 cm. These rocks are classified as tinguaites (Freudenberg, 1906; Table 1). In contrast, a more leucocratic and coarser grained group with a reddish or grey colour are referred to as alkali feldspar syenite dykes (Table 1; compare Stähle et al., 2002). They have widths of 1–5 cm, rarely up to 40 cm. According to Frenzel (1975), tinguaites generally represent the older dyke generation, followed by an alternating production of alkali feldspar syenite dykes and magnetite veins. Some of the alkali feldspar syenites show a complex internal structure that might indicate several dyke generations. In some samples, a tinguaite can be found in their inner part. As a consequence of this close spatial and temporal relationship between the different groups of dykes, a clear categorization is not always possible. Moreover, intermediate rock types exist (e.g. sample Kb50, see below).

3.3.1. Tinguaites (samples KbU5, KbU6, Kb31)

Major components of the tinguaites are alkali feldspar and different modal proportions of altered foid minerals, aegirine, amphibole, Fe–Ti oxides and apatite. They may show a fluidal texture with an inhomogeneous distribution of the major mineral phases (Fig. 3a). Accessory minerals include sphalerite, pyrite and some unidentified Nb–Zr–Ti oxides. In the inner part of the dykes, lense-shaped voids with a secondary filling of zeolite minerals (natrolite), secondary aegirine needles, recrystallized alkali feldspar, Fe-sulfides (mostly pyrite), monazite and unidentified Zr-silicates indicate a late-magmatic fluid circulation.

One porphyritic tinguaite sample (Kb31) with higher contents of mafic phases and feldspathoid minerals is regarded as the earliest and least evolved among the investigated tinguaites. It contains large nepheline phenocrysts that are embedded in a groundmass of fibrous aegirine and alkali feldspar. Sector-zoned biotite, apatite, strongly altered Fe–Ti oxides and foid minerals are microphenocrystic components. Based on its mineral assemblage and texture, this sample possibly represents a rock type intermediate between phases I and II, thus indicating a continuous magmatic evolution of the various Katzenbuckel melts.

3.3.2. "*Normal*" alkali feldspar syenite dykes (samples KbU4, Kb47, Kb50)

These rocks predominantly consist of medium to coarse-grained framework-forming alkali feldspar, with only minor amounts of altered euhedral feldspathoid minerals. Aegirine, amphibole, biotite and Fe–Ti oxides occur in varying proportions with aegirine often overgrowing amphibole (Fig. 3b). The dykes are often symmetrically zoned possibly indicating successive magmatic events (see Table 1, samples Kb47 and KbU4, each showing an outer (dyke1) and an inner (dyke2) zone). In some cases, different generations can clearly be distinguished (Kb47) whereas in other cases their separation is less distinct (KbU4, Fig. 3e). At the contact to the host rock (fallback breccia), dyke1 of sample KbU4 is medium grained with a very high content of alkali feldspar. Anhedral biotite overgrowing Fe–Ti oxides dominates among the mafic minerals. Subhedral clinopyroxene, strongly corroded grains of apatite and altered foid minerals are subordinate. The boundary towards the inner dyke2 is marked by a general increase in grain size and the appearance of large crystals of aegirine and amphibole instead of biotite. In a narrow zone, tabular alkali feldspar is oriented perpendicular to the dyke axis (Fig. 3e). Magnetite, partly with a skeletal texture (Fig. 3c), ilmenite and occasionally euhedral foid minerals can be found in between. Alkali feldspar and aegirine show discontinuous growth rims of a later mineral generation. The inner part of the dyke is filled with a dense green to brown and partly zeolitized groundmass. It consists of aegirine and amphibole needles and contains randomly oriented alkali feldspar and amphibole phenocrysts. Both euhedral and anhedral apatite can be found in the inner dyke2. Fe–Ti oxides are strongly altered.

The mineral assemblage of sample Kb50 slightly differs from the typical alkali feldspar syenites in having a higher aegirine and a lower alkali feldspar content. With respect to its low foid content, coarse grain size and

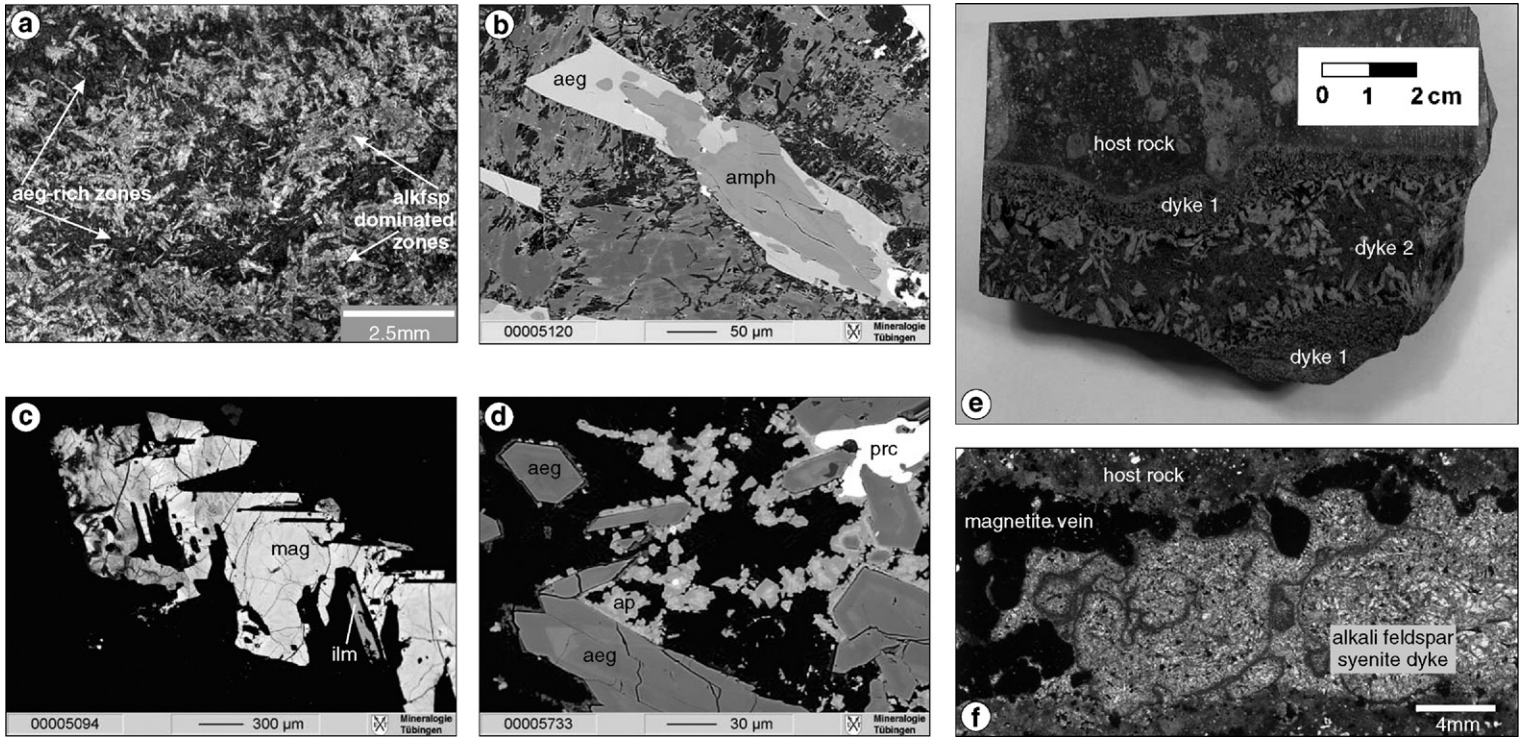

Fig. 3. Petrographic features of phase II rocks from the Katzenbuckel. (a) Fluidal texture with an inhomogeneous distribution of the major minerals in a tinguaite dyke (KbU6): fine-grained aegirine-rich zones alternate with more coarse-grained areas dominated by alkali feldspar. (b) Relics of amphibole overgrown by aegirine, embedded in partly zeolitized alkali feldspar in an alkali feldspar syenite dyke (Kb48, BSE image). (c) Ti-rich magnetite with a sceletal growth and subordinate ilmenite from KbU4dyke2; the BSE image reveals strong corrosion textures at the margins of the crystals. (d) Anhedral, late-magmatic apatite and pyrochlore (prc) overgrowing zoned crystals of aegirine in the alkali feldspar syenite dyke Kb48 (BSE image). (e) Symmetrically zoned alkali feldspar syenite dykes of sample KbU4 showing an outer (dyke1) and an inner (dyke2) zone. The host rock in this case is the fallback breccia consisting of sedimentary fragments, lapilli and volcanic bombs. (f) Alkali feldspar syenite dyke (Kb49) associated with magnetite veins showing exsolution textures.

strongly parallel oriented fabric caused by the feldspar laths and fibrous aegirine, however, it resembles more the alkali feldspar syenites than the tinguaites. Amphibole usually intergrown with or overgrown by aegirine and corroded and exsolved magnetites are minor phases. Additionally, sample Kb50 shows a broad variety of rare accessory minerals often being concentrated along thin ribbon-like zones. These include anhedral monazite and pyrochlore, tabular freudenbergite (up to 100 μm) with aegirine or hematite and various Na–Ti–Nb-silicates (predominantly lorenzenite).

3.3.3. Alkali feldspar syenite dykes associated with magnetite veins (Kb48, Kb49)

A group of red coloured alkali feldspar syenite dykes is closely related to magnetite veins either cutting and intruding them or even partly mixing with them (Fig. 3f). Principally, they show the same assemblage as the typical alkali feldspar syenite dykes. The most significant deviations are the absence of biotite and the Fe–Ti oxide assemblage. Ilmenite is most abundant. It may exsolve hematite or is intergrown with it or with a Nb–Fe–Ti oxide (possibly freudenbergite) and aegirine. Former Ti-rich magnetite has been exsolved to magnetite and ilmenite showing trellis-type exsolution textures (after the terminology of Buddington and Lindsley, 1964). Euhedral zircon and subordinate anhedral carbonates, pyrochlore and late apatite occur as accessory minerals (Fig. 3d). The associated magnetite veins consist mainly of unexsolved magnetite with minor amounts of carbonates, apatite and clinopyroxene and clusters of monazite. Additionally, Frenzel (1975) observed veins dominated by apatite.

3.4. Metasomatic alteration features (samples KbU2, Kb48, Kb49)

Both rock types of phase I occur also as metasomatically altered varieties (see also Freudenberg, 1906; Frenzel, 1955). Alteration zones are particularly developed in the phonolite close to the contact with the nepheline syenite body. A characteristic feature of these altered varieties is their reddish colour. The investigated sample KbU2 has a slightly porphyritic texture, with clinopyroxene and nepheline as phenocryst phases. In contrast to the unaltered phonolites, the clinopyroxenes are intensively corroded. Microphenocrystic nepheline, alkali feldspar and a precursor sodalite group mineral are strongly replaced by zeolithes. Neither amphibole nor biotite is present. Aggregates of fine-grained hematite with clinopyroxene and rimmed by alkali feldspar with hematite inclusions replace euhedral crystals (Fig. 2f), which we interpret as precursor olivine. The most characteristic feature of the altered phonolite, however, is the replacement of magnetite and ilmenite by pseudobrookite and hematite (Fig. 2g and h).

The two main rock types have also undergone alteration in the neighboring areas of magnetite veins (samples Kb48 and Kb49). Of the primary assemblage, only apatite and clinopyroxene remained. Besides abundant zeolites that replace precursor foid minerals, numerous small clustered clinopyroxenes are present in the fine-grained brown groundmass. Irregularly shaped cavities are filled with titanian andradite that can also replace magnetite. To a lesser extent, carbonates appear as secondary phases.

4. Mineral chemistry

4.1. Analytical methods

Minerals were analyzed with a JEOL 8900 electron microprobe in wavelength-dispersion mode at the Institut für Geowissenschaften, Universität Tübingen (Germany), using a beam current of 15 nA and an acceleration voltage of 15 kV. The counting time on the peak was 16 s for major elements, 30–60 s for minor elements (Mn, Ba, Zr, Cl, F). Background counting times were half of the peak counting times. To avoid Na migration under the electron beam, silicates were analyzed using a defocused beam of 5 μm diameter. For calibration, both natural and synthetic mineral phases were used as standards. Processing of the raw data was carried out with the internal ϕρZ correction method of JEOL (Armstrong, 1991).

4.2. Feldspar

The Katzenbuckel feldspars are essentially Ca-free ($CaO < 0.23$ wt.%), but contain elevated amounts of iron (Fe_2O_3 between 0.5–2.8 wt.%) and Ba (up to 5.7 wt.% BaO; Table 2). All iron was calculated as Fe^{3+} (Deer et al., 1963, 1992) and is expressed as FeOr ($KFe^{3+}Si_3O_8$) component, which reaches up to 10 mol% in some of the dyke rocks and in the metasomatically altered phonolite. For most analyses, Fe^{3+} p.f.u. shows a negative 1 : 1 correlation with Al p.f.u. (Fig. 4a). Feldspars, which show a deviation from this main trend towards higher Al values, are enriched in Ba, containing between 2.0 and 5.65 wt.% BaO. In these cases, the Fe^{3+}–Al exchange is partly camouflaged by the coupled incorporation of Al and Ba. In phonolites and nepheline syenites, the composition varies between

Table 2
Representative microprobe analyses of feldspars and nephelines from the Katzenbuckel

Mineral	Fsp	Fsp	Fsp	Fsp	Fsp	Fsp	Fsp	Ne	Ne	Ne	Ne
Sample	Kb3	Kb24	Kb31	KbU4dyke2	Kb50	Kb48		Kb3	Kb24	Kb25	KbU2
Rock type	Phonolite	Nepheline syenite	Tinguaite	Alkali feldspar syenite dyke	Metasom. altered alkali feldspar syenite dyke	Alkali feldspar syenite dyke associated with magnetite veins		Phonolite	Nepheline syenite	Nepheline syenite	Metasom. altered phonolite
wt.%											
SiO_2	64.87	60.61	65.33	63.98	65.36	66.82	65.50	45.98	43.90	42.74	45.54
$Al2O_3$	18.12	19.54	17.30	17.84	16.87	17.63	18.14	30.31	31.55	32.70	30.67
Fe_2O_3	0.83	0.76	1.27	1.32	2.76	1.68	0.26	1.52	1.20	0.80	2.62
CaO	0.01	0.05	0.00	0.05	0.02	0.03	0.00	0.11	0.01	0.22	0.04
BaO	0.78	5.67	0.07	1.51	0.10	0.21	0.08	0.00	0.05	0.08	0.00
Na_2O	2.90	3.73	1.74	1.64	3.94	7.10	0.40	16.15	16.17	16.91	16.90
K_2O	11.96	8.86	14.45	13.70	10.92	6.82	16.50	5.19	6.41	5.73	4.98
Total	99.47	99.22	100.16	100.04	99.97	100.29	100.88	99.25	99.28	99.17	100.75
	Formulae based on 8 (feldspar) and 32 (nepheline) oxygens										
Si	2.99	2.88	3.01	2.98	3.00	3.00	3.01	8.85	8.53	8.31	8.68
Al	0.99	1.10	0.94	0.98	0.91	0.93	0.98	6.87	7.22	7.50	6.89
Fe^{3+}	0.03	0.03	0.04	0.05	0.10	0.06	0.01	0.22	0.18	0.12	0.38
Ca	0.00	0.00	0.00	0.00	0.00	0.00	0.00	0.02	0.00	0.05	0.01
Na	0.26	0.34	0.16	0.15	0.35	0.62	0.04	6.02	6.09	6.38	6.25
K	0.70	0.54	0.85	0.81	0.64	0.39	0.97	1.27	1.59	1.42	1.21
Ba	0.01	0.11	0.00	0.03	0.00	0.00	0.00	0.00	0.00	0.01	0.00
Sum	4.98	5.00	5.00	5.00	5.00	5.00	5.01	23.25	23.61	23.79	23.42
mol%											
Ab	27	39	16	15	35	61	4	Ne 68	71	78	72
An	0	0	0	0	0	0	0	Ks 15	19	17	14
Or	70	58	80	80	55	33	95	Qtz 17	10	5	14
FeOr	3	3	4	5	10	6	1				

$Or_{48–81}FeOr_{2–8}Ab_{16–46}$. Feldspars from tinguaites have high sanidine contents ($Or_{80–99}FeOr_{0–8}Ab_{0–16}$) and feldspars from the alkali feldspar syenite dykes vary in composition between $Or_{45–97}FeOr_{0–10}Ab_{2–48}$. The widest compositional range reaching the highest Ab contents – $Or_{33–96}FeOr_{1–9}Ab_{3–61}$ – was found in the alkali feldspars syenite dykes associated with magnetite veins.

4.3. Nepheline

Due to complete alteration of nepheline in the dyke rocks, nepheline composition could only be analyzed in the phase I rocks. The composition ranges from $Ne_{78}Ks_{17}Qtz_5$ to $Ne_{68}Ks_{15}Qtz_{17}$ (Table 2). Generally, the compositional range is relatively narrow and no chemical zonation was found in phenocrysts nor was a chemical difference between early and late crystals detected. Minor elements are Ca (CaO < 0.77 wt.%) and Ba (BaO < 0.10 wt.%). Fe_2O_3 contents vary between 0.76 and 2.63 wt.% with the highest concentrations in the metasomatically altered phonolite. Fig. 4b shows a roughly negative correlation between Fe^{3+} and Al. Full tetrahedral occupancy (16 atoms per formula unit) is only reached if Fe^{3+} is added to the sum of Si + Al (Table 2).

4.4. Olivine

Olivine composition varies between $Fo_{78}Fa_{21}Tp_1$ and $Fo_{68}Fa_{30}Tp_2$ (Table 3). The highest Fa contents were detected in olivine relics overgrown by biotite in the phonolite whereas the highest Fo contents were found in olivine inclusions in nepheline phenocrysts of the nepheline syenites. MnO contents, being positively correlated with Fa-content, range between 0.84 and 1.53 wt.% and CaO between 0.12 and 0.39 wt.% CaO, showing a slight negative correlation with Fe^{2+}. Ni is generally below 200 ppm. No chemical zonation in individual olivine grains was observed.

4.5. Clinopyroxene

In most samples two generations of clinopyroxene are present: large phenocrysts and groundmass miner-

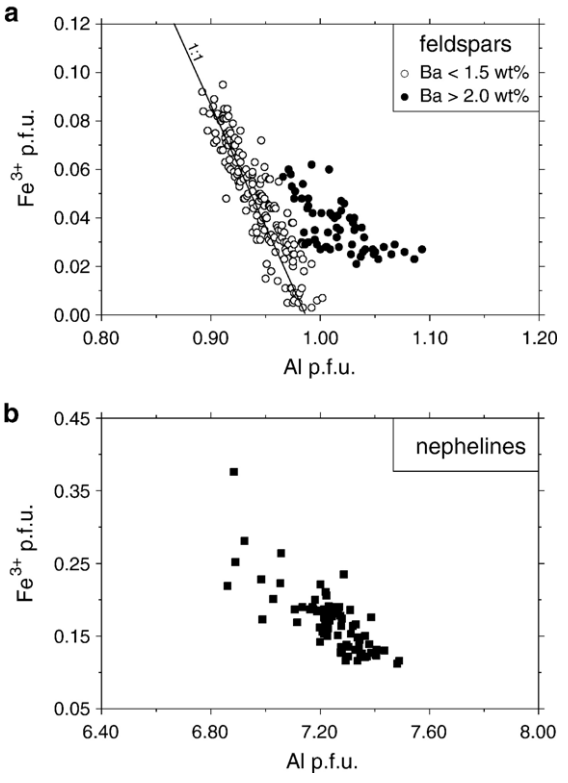

Fig. 4. Correlation diagrams of Fe^{3+} p.f.u. and Al p.f.u. for the Katzenbuckel feldspars (a) and nephelines (b).

als. Representative analyses are shown in Table 4. For a detailed chemical classification, eight endmembers were used. Calculated amounts of these components in the various Katzenbuckel rocks are summarized in Table 5 and details on the endmember calculations are given in Appendix A.

Besides the classical Quad-components (enstatite (En), ferrosilite (Fs), diopside (Di) and hedenbergite (Hd)), the most important Na-component is aegirine (Aeg), whereas jadeite (Jd) plays only a limited role. However, in most analyses, Na-content exceeds the calculated ($Fe^{3+}Al_{oct}$), implying additional Na-components. Excess Na (expressed in terms of [Na − (Fe^{3+} + Al_{oct})]) shows a positive correlation with the sum of [Ti+Zr] (Fig. 5a). The proportion of about 2 : 1 implies the existence of a Ti- and Zr-bearing sodic pyroxene component with the general formula Na(Ti, Zr)$_{0.5}$(Mg, Fe^{2+})$_{0.5}Si_2O_6$, here referred to as (Ti, Zr)-aegirine ((Ti, Zr)-Aeg). This component is already known from other alkaline igneous rock suites worldwide (e.g., Ranløv and Dymek, 1991; Larsen, 1976; Ferguson, 1977; Grapes et al., 1979; Nielsen, 1979). Most analyses, however, contain more [Ti+Zr] than necessary to form (Ti, Zr)-Aeg. Expressed as $[Ti+Zr]_{rest}$, this excess shows a strong correlation with Al_{tetr} with a proportion of 1 : 2 (Fig. 5b). As Ca must be incorporated in this endmember, the amount of Ca available apart from the formation of Di, Hd is expressed as $[Ca–M^{2+}]_{rest}$ with M^{2+} = Mg + Fe^{2+} + Mn. In Fig. 5c, this difference is plotted against Al_{tetr}. Ca–Ti or Ca–Zr tschermakite components (Ca-(Ti, Zr)Al_2O_6) that meet the observed (Ti+Zr) : Al_{tetr} ratio but would also require a Ca : Al_{tetr} ratio of 1 : 2 are well known from other localities (Larsen, 1976; Njonfang and Nono, 2003; Coulson, 2003). As the latter proportion clearly exceeds 1 : 2 but approaches about 1 : 1 for the Katzenbuckel pyroxenes (Fig. 5c), we postulate the multi-endmember component Ca-(Ti, Zr)$_{0.5}$(Mg, Fe^{2+})$_{0.5}AlSiO_6$ and refer to it as Ca-(Ti, Zr)-component.

Both Ti- and Zr-contents reach exceptionally high values in the Katzenbuckel pyroxenes (up to 8.49 wt.% TiO_2 and up to 6.24 wt.%. ZrO_2) Generally, Ti- and Zr-contents increase from early to later rock types and groundmass pyroxenes are generally richer in Ti or Zr than phenocryst pyroxenes. In most analyses, Ti dominates over Zr, but the relationship between Ti and Zr in the Katzenbuckel pyroxenes is rather complex, showing both negative and positive correlations in various samples.

Fig. 6 shows the different endmember proportions for the Katzenbuckel rocks in comparison with published trends from other peralkaline suites. The phonolites and nepheline syenites cover a broad compositional range starting with high Di (up to 73 mol%; Table 5) to high Aeg (maximum of 63 mol%) without any significant enrichment of the Hd component (<15 mol%) during fractionation (Fig. 6a). Pyroxenes from the metasomatized phonolite sample (KbU2) reveal a shift towards even lower Fe^{2+} contents. A similarly large range is covered by the alkali feldspar syenite dykes KbU4 and Kb47 (Table 5) with primitive compositions in the outer dyke generations (dyke1) and a strong increase in Aeg component towards the inner part of dyke2, respectively. Intermediate compositions are represented by phenocrysts from the inner boundary of KbU4dyke2. The tinguaites and the alkali feldspar syenite dykes associated with magnetite veins contain more evolved clinopyroxenes starting with a minimum of about 30 mol% Aeg (Fig. 6a). Compared with trends from other localities (dashed lines), the Katzenbuckel pyroxenes show an almost unique trend as they show almost no increase of Fe^{2+} during fractionation, whereas most other trends indicate an initial increase in Hd, before bending towards Aeg.

Table 3
Representative microprobe analyses of olivines and Fe–Ti oxides from the Katzenbuckel

Mineral	ol	Ol	Ol	mag	mag	mag	mag	ilm	ilm	Hem	hem	psbrook	psbrook
Sample	Kb3	Kb24	Kb22	Kb25	Kb49	Kb48	Kb49	Kb3	Kb49	KbU2	KbU2	KbU2	KbU2
Rock type	Phonolite	Nepheline syenite	Nepheline syenite	Nepheline syenite	Alkfsp syenite dyke with magnetite veins	Magnetite vein	Magnetite vein	Phonolite	Alkfsp syenite dyke with magnetite veins	Metasomatically altered phonolite			
wt.%													
SiO_2	37.52	38.27	39.28	–	–	–	–	–	–	–	–	–	–
TiO_2	0.06	0.12	0.04	18.86	10.27	0.84	2.74	51.44	48.74	12.25	16.61	44.21	44.72
Al_2O_3	0.01	0.02	0.02	0.85	0.06	0.76	5.29	0.02	0.01	0.12	0.22	0.32	0.53
Cr_2O_3	–	–	–	0.02	0.05	0.08	0.00	0.00	0.00	0.03	0.00	0.10	0.00
Fe_2O_3 (calc.)*				33.01	49.16	67.74	59.16	6.67	7.77	80.45	70.58	48.88	47.96
FeO (calc.)*	26.82	21.88	20.37	40.88	34.28	25.97	21.77	34.42	24.17	0.96	6.94	0.00	0.00
MnO	1.43	1.27	1.06	1.70	4.11	3.23	6.69	2.13	17.21	1.27	0.96	0.49	0.52
MgO	34.38	38.58	39.77	3.73	0.62	1.82	3.38	5.43	0.54	4.79	3.87	5.34	5.45
CaO	0.12	0.25	0.39	–	–	–	–	–	–	–	–	–	–
ZnO	–	–	–	0.25	1.35	0.26	0.79	0.00	1.47	0.27	0.14	0.00	0.09
Total	100.34	100.39	100.93	99.30	99.90	100.70	99.82	100.11	99.91	100.14	99.32	99.34	99.27
	Formulae based on 4 oxygens			Formulae based on ideal cation–oxygen ratios: 3:4 (mag), 2:3 (ilm, hem), 3:5 (psbrook)									
Si	1.00	0.99	1.01	–	–	–	–	–	–	–	–	–	–
Al	0.00	0.00	0.00	0.04	0.00	0.03	0.23	0.00	0.00	0.00	0.01	0.01	0.02
Ti	0.00	0.00	0.00	0.52	0.29	0.02	0.08	0.94	0.93	0.23	0.32	1.26	1.28
Cr	–	–	–	0.00	0.00	0.00	0.00	0.00	0.00	0.00	0.00	0.00	0.00
Fe^{3+}				0.91	1.41	1.91	1.62	0.12	0.15	1.53	1.36	1.45	1.42
Mg	1.37	1.49	1.52	0.21	0.04	0.10	0.18	0.20	0.02	0.18	0.15	0.30	0.31
Fe^{2+}	0.60	0.48	0.44	1.26	1.09	0.81	0.66	0.70	0.51	0.02	0.15	0.00	0.00
Mn	0.03	0.03	0.02	0.05	0.13	0.10	0.21	0.04	0.37	0.03	0.02	0.02	0.02
Ca	0.00	0.01	0.01	–	–	–	–	–	–	–	–	–	–
Zn	–	–	–	0.01	0.04	0.01	0.02	0.00	0.03	0.00	0.00	0.00	0.00
Sum	3.00	3.00	3.00	3.00	3.00	2.98	3.00	2.00	2.01	1.99	2.01	3.04	3.05
mol%													
Fo or usp/ilm	68	75	77	53	29	2	8	94	93	23	32		
Fa or mag/hem	30	24	22	47	71	98	92	6	7	77	68		
Tp	2	1	1										

(calc.)*: calculated FeO and Fe_2O_3 contents are based on microprobe analyses assuming stoichiometry. – not analyzed.

The increase in Aeg component is generally accompanied by an increase in (Ti, Zr)-Aeg (Fig. 6b). In the late-stage or groundmass pyroxenes, the (Ti, Zr)-Aeg content can reach maximum values >40 mol% (Table 5). In aegirines from the tinguaites, the (Ti, Zr)-Aeg content is constantly high, while in Kb48 and Kb49 a slight increase of (Ti, Zr)-Aeg can be observed in the latest pyroxenes (Fig. 6b).

The Ca-(Ti, Zr)-component (Fig. 6c) reaches up to 16 mol% and is highest in the metasomatized phonolite and in the unaltered phonolites and nepheline syenites (Table 5). While (Ti, Zr)-Aeg shows an increase during fractionation, the Ca-(Ti, Zr)-component is present at a low but relatively constant level that is similar in pyroxenes from all rock types.

4.6. Fe–Ti oxides

The compositional variation of Fe–Ti oxides is presented in the $FeO–Fe_2O_3–TiO_2$ triangle (Fig. 7), where MgO and MnO were added to FeO and Table 3 shows representative analyses. Due to strong alteration, compositions of magnetites could not be determined in all samples. Furthermore, semi-quantitative detection revealed some Nb–Fe–Ti oxides and elevated Nb contents in some ilmenites, particularly in some tinguaites and alkali feldspar syenite dykes. These analyses were neglected in this study.

Ti contents of homogeneous magnetites are highest in nepheline syenites ($Usp_{55–38}Mag_{45–62}$) and

Table 4
Representative microprobe analyses of clinopyroxenes from the Katzenbuckel

Sample	Kb24	KbU6	Kb25	KbU2	Kb31	KbU6	Kb47dyke1	KbU4dyke2	Kb49	Kb48
Rock type	Nepheline syenite	Nepheline syenite	Nepheline syenite	Metasom. Altered phonolite	Tinguaite	Tinguaite	Alkali feldspar syenite dyke		Alkali feldspar syenite dyke associated with magnetite veins	
wt.%										
SiO_2	49.49	52.54	50.73	51.16	52.16	52.44	51.22	52.38	52.44	50.82
TiO_2	2.84	1.88	8.49	1.62	4.08	4.35	1.48	5.77	1.54	4.88
Al_2O_3	3.69	0.52	0.74	2.27	0.92	0.58	2.17	0.52	0.73	1.04
Fe_2O_3 (calc.)*	4.02	15.74	16.92	6.50	12.22	24.52	2.73	22.02	12.35	17.08
FeO (calc.)*	3.47	2.22	4.08	0.00	5.23	1.46	3.26	1.91	3.50	1.21
MnO	0.27	0.42	0.28	0.24	0.36	0.25	0.17	0.28	1.14	0.27
MgO	13.40	7.10	2.49	14.57	6.14	2.03	14.35	1.71	8.39	4.09
CaO	21.44	10.38	2.25	21.78	9.13	1.76	22.80	0.52	11.34	2.08
Na_2O	1.45	7.97	12.30	1.86	8.25	12.79	0.95	13.43	6.65	12.36
K_2O	0.01	0.01	0.05	0.00	0.00	0.02	0.00	0.00	0.03	0.01
ZrO_2	0.18	1.84	0.97	0.11	0.77	0.54	0.06	0.61	1.68	6.24
Total	100.26	100.62	99.30	100.11	99.26	100.74	99.19	99.15	99.79	100.08
	Formulae based on 4 cations and 6 oxygens									
Si	1.84	1.98	1.94	1.88	1.98	1.97	1.91	1.99	1.98	1.93
Al	0.16	0.02	0.03	0.10	0.04	0.03	0.10	0.02	0.03	0.05
Fe^{3+}	0.11	0.44	0.49	0.18	0.35	0.69	0.08	0.63	0.35	0.49
Ti	0.08	0.05	0.24	0.04	0.12	0.12	0.04	0.17	0.04	0.14
Zr	0.00	0.03	0.02	0.00	0.01	0.01	0.00	0.01	0.03	0.12
Mg	0.74	0.40	0.14	0.80	0.35	0.11	0.80	0.10	0.47	0.23
Fe^{2+}	0.11	0.07	0.13	0.00	0.17	0.05	0.10	0.06	0.11	0.04
Mn	0.01	0.01	0.01	0.01	0.01	0.01	0.01	0.01	0.04	0.01
Ca	0.85	0.42	0.09	0.86	0.37	0.07	0.91	0.02	0.46	0.08
Na	0.10	0.58	0.91	0.13	0.61	0.94	0.07	0.99	0.49	0.91
K	0.00	0.00	0.00	0.00	0.00	0.00	0.00	0.00	0.00	0.00
Sum	4.00	4.00	4.00	4.00	4.01	4.00	4.02	4.00	4.00	4.00
Di	60	33	3	76	23	2	73	0	34	3
Hd	9	7	3	1	12	1	10	0	10	1
En	4	0	0	0	1	0	2	0	4	0
Fs	1	0	0	0	1	0	0	0	1	0
Aeg	10	44	49	13	35	70	7	63	35	49
Jd	0	0	0	0	2	0	0	2	1	0
Ti-Aeg	0	14	42	0	24	24	0	34	13	42
Ca-(Ti, Zr)-comp.	16	2	3	10	2	3	8	1	2	5

lowest in the late magnetite veins ($Usp_{15-2}Mag_{85-98}$). Exsolved magnetites in alkali feldspar syenite dykes have intermediate compositions of about $Usp_{33}Mag_{67}$ (Kb49) and about $Usp_{15}Mag_{85}$ (Kb48), respectively. Al_2O_3 contents are generally low (<0.9 wt.%) in both exsolved and unexsolved magnetites, but reach 5.3 wt.% in the late magnetite veins. MgO and MnO contents reach up to 3.7 and 6.9 wt.%, respectively.

The composition of both homogeneous and exsolved ilmenites range between $Ilm_{95}Hem_5$ and $Ilm_{89}Hem_{11}$. Al_2O_3 is always below 0.06 wt.%, but elevated Mg (up to 6.0 wt.% MgO) and Mn contents (up to 21.8 wt.%) were detected.

The secondary Fe–Ti oxides of sample KbU2 show relatively high contents of MgO (pseudobrookites: ~5.3 wt.%; hematites ~4.9 wt.%) but low contents of MnO (pseudobrookites: ~0.5 wt.%; hematites ~1.3 wt.%) both of which were present in elevated concentrations in the primary magnetite–ilmenite assemblage. TiO_2 reaches 16.6 wt.% in hematites resulting in compositions of $Ilm_{20-32}Hem_{80-68}$. With an average composition of $Mg_{0.3}Fe^{3+}_{1.4}Ti_{1.3}O_5$, the Katzenbuckel pseudobrookites (compare Ottemann and Frenzel, 1965) belong to a solid solution series between ideal pseudobrookite ($Fe^{3+}Fe^{3+}TiO_5$) and the Mg-endmember ($Mg_{0.5}Fe^{3+}Ti_{1.5}O_5$; Bowles, 1988).

Table 5
Clinopyroxene endmember proportions (mol%) in the various Katzenbuckel rock types

		En	Fs	Di	Hd	Quad	Ac	Jd	Ti-Aeg	Ca-(Ti, Zr)-comp.
Phonolite	Phenocrysts	3–4	0–1	63–69	9–12	78–82	8–9	0–1	0	9–11
	Matrix	2–4	0–1	49–67	7–12	60–78	11–28	0–4	3–9	1–6
Nepheline syenite	Phenocrysts	0–7	0–2	33–73	5–14	40–87	2–44	0–4	0–14	1–16
	Matrix	0–5	0–1	3–71	1–15	5–89	2–63	0–7	1–42	0–10
Metasom. altered phonolite	Phenocrysts	0–3	0	54–75	1–9	58–81	11–35	0–1	0–3	6–16
	Matrix	1–4	0	43–72	1–4	48–75	17–39	0–1	0–9	4–10
Tinguaites		0–1	0–1	2–28	1–12	4–42	35–69	0–8	14–26	0–4
Alkali feldspar syenite dykes	KbU4dyke1, Kb47dyke1	2–6	0–1	56–73	6–14	71–88	4–20	0–5	0–7	0–8
	KbU4dyke2, Kb47dyke2,Kb50	0–3	0–2	0–52	0–19	0–73	17–73	0–4	5–41	0–4
	Kb48, Kb49: contact to magnetite vein	2–10	0–5	11–33	3–13	20–59	31–57	0–2	7–25	0–4
	Kb48, Kb49: dyke centres and late cpx generation	0–6	0–2	0–30	0–9	0–47	38–82	0–8	7–42	0–5

Quad = En+Fs+Di+Hd.

4.7. Biotite

The Katzenbuckel biotites (X_{Fe} between 0.14 and 0.49) are characterized by low Al contents and 8-Si+Al deficits of 0.22–0.50 p.f.u. (Table 6), indicating the presence of tetrahedrally coordinated Fe^{3+} (e.g. Dunworth and Wilson, 1998) or Ti^{4+} (Deer et al., 1992). High Ti contents (4.3–12.8 wt.% TiO_2) are a characteristic feature of the Katzenbuckel biotites. However, all analyses reveal a strongly negative correlation between Ti and the two dominating elements on the octahedral position (Mg, Fe^{2+}; Fig. 8a). In high-Ti analyses, Mg shows a variation independent from the Fe^{2+}content. Wagner et al. (1987), proposed the coupled substitution of $Mg^{2+}+2\ Si^{4+}<->Ti^{4+}+2\ Al^{3+}$ for a single Katzenbuckel nepheline syenite. The observed positive correlation between Ti and Al with a proportion of about 1:2 in the investigated biotites of our work support this assumption (Fig. 8b). A further possibility for reaching charge balance while replacing divalent cations by Ti^{4+} on octahedral sites might be the creation of vacancies on the *X* position (Deer et al., 1992) of the mica structure ($Mg^{2+}+2\ K^{+}<->Ti^{4+}+2\bullet\square$). According to the applied formula calculation up to about 10% of the *X* position may be vacant.

As common in biotites from alkaline rocks especially from K-poor rock types (Dunworth and Wilson, 1998) elevated Ba contents (up to 3.1 wt.% BaO) were detected and show a positive correlation with Ti (Fig. 8c). For the occupation of the hydroxyl sites, Cl is unimportant (<0.1 wt.%), but F contents range between 0.2 and 2.4 wt.%. F and Fe and F and Ti contents are negatively correlated in all samples.

Sector-zoning is a typical feature of the euhedral biotites of the nepheline syenite Kb25 and the tinguaite Kb31 (see also Wagner et al., 1987). Fig. 9 shows the BSE image of a biotite with a complex internal zoning structure and a second generation. Positive correlation trends exist between Si, Mg, F and K on the one hand and Ti and Ba on the other. Ba values are high in sector I and decrease stepwise when crossing the border to sectors II and III, with rather constant concentrations within one specific sector. For the other elements, the changes are more continuous within sectors I–III. At the border to the later growth rim (profile C–D) some elements show a sharp increase (Ba, Mg, F), whereas others indicate a more continuous change (K, Si, Ti).

4.8. Amphibole

Some representative amphibole analyses are shown in Table 6. Based on the nomenclature of Leake et al. (1997), the analyzed amphiboles fall in two groups: sodic–calcic amphiboles (richterite to magnesiokatophorite) and sodic amphiboles (magnesio-arfvedsonitie to ferric-nyböite). The dominant substitution mechanism seems to be the coupled substitution of $Na^{+}+Fe^{3+}<->Ca^{2+}+(Mg,\ Fe)^{2+}$, describing the transition from the sodic–calcic to the sodic amphibole members. X_{Mg} in the Katzenbuckel amphiboles is always >0.5.

As for biotites, the Katzenbuckel amphiboles are characterized by relatively low Al contents (0.76–3.4

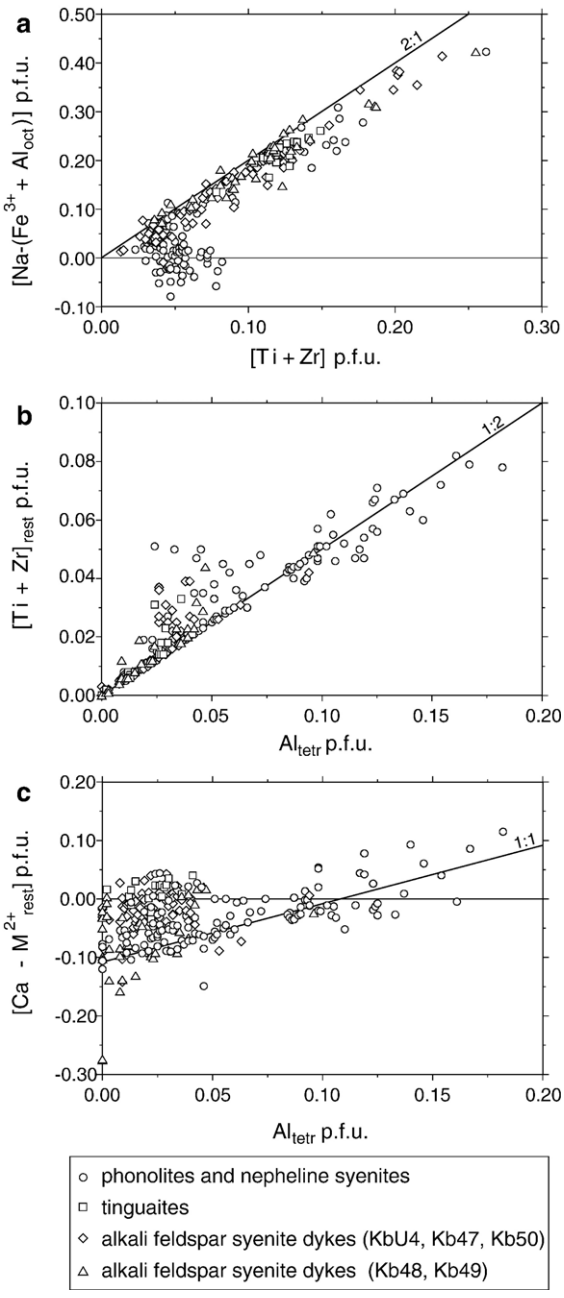

Fig. 5. Correlation diagrams for Katzenbuckel pyroxenes. (a) Excess Na (expressed in terms of $[Na-(Fe^{3+}+Al_{oct})]$ shows an approximate 2:1 correlation with the sum of [Ti+Zr] indicating the existence of the (Ti, Zr)-aegirine endmember. (b) Excess $[Ti+Zr]_{rest}$ shows a strong correlation with Al_{tetr} with a proportion of 1:2. (c) $[Ca–M^{2+}]$ with $M^{2+}=Mg+Fe^{2+}+Mn$ against Al_{tetr} indicating the existence of a multi-endmember component Ca-(Ti, Zr)$_{0.5}$(Mg, Fe^{2+})$_{0.5}AlSiO_6$ (see text for detailed discussion).

wt.% Al_2O_3) and calculated 8-Si+Al deficits of up to 0.3 p.f.u., indicating tetrahedrally coordinated Ti^{4+} (Oberti et al., 1992; Della Ventura et al., 1991) or Fe^{3+} (Hogarth et al., 1987).

K_2O contents in both groups are similar, ranging from 0.99–2.8 wt.%. Among the minor elements, Mn varies between 0.1 and 1.8 wt.% MnO, showing a negative correlation with X_{Mg}. ZrO_2 contents reach up to 1.3 wt.%, showing no systematic relation to Ti. F contents vary between 0.07 and 2.60 wt.%, whereas Cl concentrations are always below 0.02 wt.%.

5. Calculation of intensive crystallization parameters

At a given depth of emplacement, the evolution of the Katzenbuckel melts is mainly governed by T, a_{SiO_2}, and f_{O2}. Minimum liquidus temperatures for some samples of phase I could be estimated by the use of nepheline thermometry after Hamilton (1961). Solidus temperatures, silica activity and oxygen fugacity were calculated for one phonolite (Kb3) and two nepheline syenites (Kb24, Kb25) from the assemblage of olivine, clinopyroxene, ilmenite and magnetite using the QUILF program of Andersen et al. (1993). In the dyke rocks of phase II, such calculations were not possible due to either the lack of a suitable phase assemblage or because of the strong alteration of relevant mineral phases. Detailed information on the theoretical background and the application of the QUILF program has been given by Lindsley and Frost (1992), Frost and Lindsley (1992) and Marks and Markl (2001). In our calculations, temperature was derived from the Fe–Mg-exchange between olivine and clinopyroxene and from two-oxide thermometry. For the calculation of silica activity and oxygen fugacity, the displaced reaction

$$FeSiO_3(\text{in augite}) + Fe_2TiO_4(\text{in magnetite}) = FeTiO_3(\text{in ilmenite}) + Fe_2SiO_4(\text{in olivine})$$

was used. In order to minimize the effects of subsoldidus cation diffusion, only the Fe-richest clinopyroxene core compositions and the average olivine values were used (Markl, 1998). Most olivine crystals were protected from later re-equilibration as they occur as inclusions in nepheline phenocrysts. Relative oxygen fugacity was determined including the whole range of Fe–Ti oxide mineral compositions for each sample.

5.1. Pressure

Based on the overlying sedimentary cover, Stähle et al. (2002) assumed a pressure of 200–300 bar for the emplacement level of the investigated rocks.

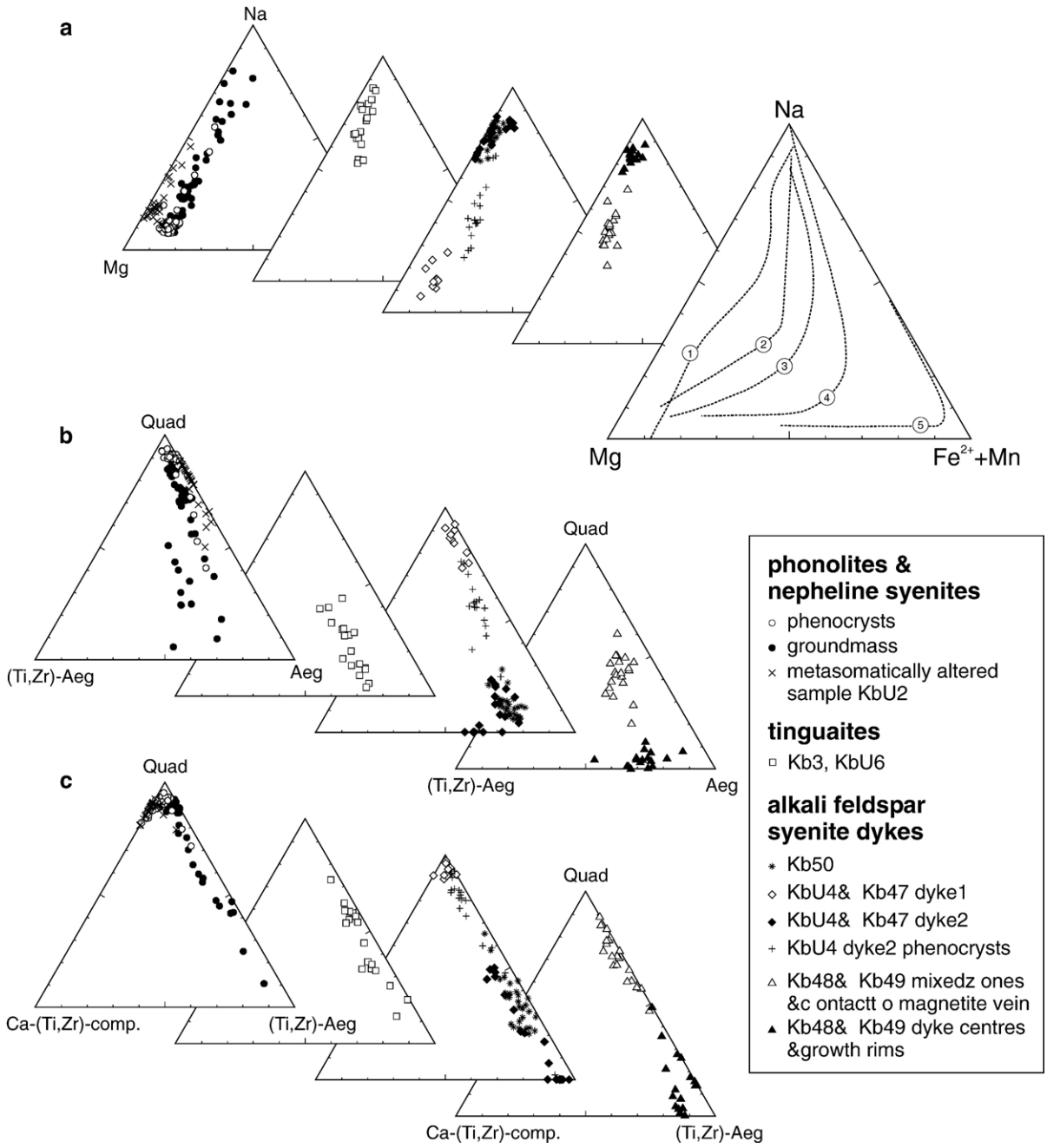

Fig. 6. Compositional variation of the Katzenbuckel pyroxenes (a) in the system Mg–(Fe^{2+}+Mn)–Na. In the right triangle pyroxene trends from other alkaline suites are shown for comparison: 1 = Murun, Siberia (Mitchell and Vladykin, 1996), 2 = Lovozero, Kola Peninsula (Korobeinikov and Laajoki, 1994), 3 = Uganda (Taylor and King, 1967), 4 = South Qoroq (Stephenson, 1972), 5 = Ilímaussaq (Larsen, 1976). (b) in the system Quad—Ti-Aeg–Aeg and (c) in the system Quad—Ca-(Ti, Zr)-comp.–Ti-Aeg. For detailed information on the endmember calculations see Appendix A.

However, the early formed phenocryts of olivine, clinopyroxene and Fe–Ti oxides used in the QUILF calculations below, probably formed at a deeper level. In accordance with typical upper crustal alkaline magma chambers (e.g., Larsen and Sørensen, 1987; Potter et al., 2004) we assume a pressure of 1 kbar. However, re-calculations with a pressure of 200 bar resulted in almost identical values.

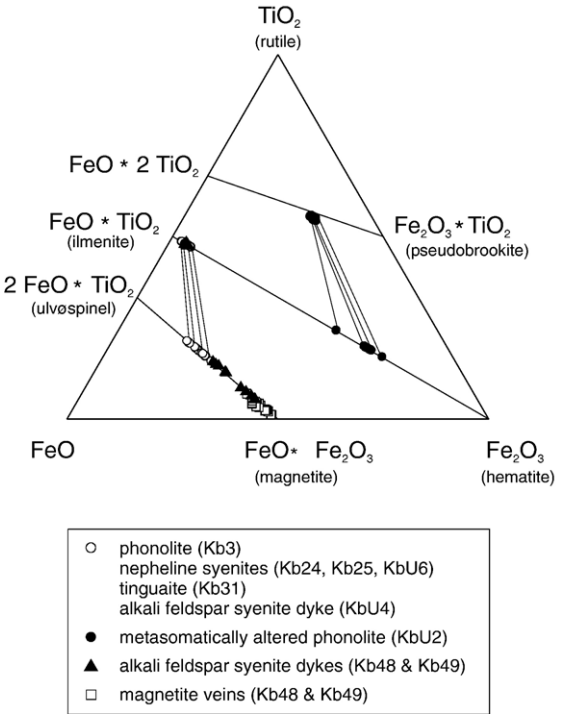

Fig. 7. The compositional variation of Fe–Ti oxides in the FeO–Fe_2O_3–TiO_2 triangle.

5.2. Temperature and silica activity

Applying nepheline thermometry after Hamilton (1961) maximum temperatures range between 750 and 780 °C. These temperatures have to be regarded as minimum liquidus temperatures, since late- to post-magmatic re-equilibration results in a Si loss and hence lower-temperature estimates (Powell, 1978).

The QUILF-calculated solidus temperatures for Kb3 and Kb24 range from 680 to 880 °C with an estimated uncertainty of about ± 20 °C (Fig. 10). In the case of sample Kb25, the application of the QUILF calculations is restricted as it lacks clinopyroxene phenocrysts and the groundmass pyroxene is enriched in Na. For this sample, a very broad temperature range reaching down to 600 °C was calculated (Fig. 10). This possibly reflects the late-stage conditions, which are in accordance with temperatures derived for the late magmatic alkali feldspar syenite dykes (between 550 and 750 °C; Stähle et al., 2002). Another constraint on temperature for the late magmatic stage is given by the secondary pseudobrookite–hematite assemblage in the metasomatically altered phonolite (KbU2) and in some of the alkali feldspar syenite dykes also investigated by Stähle et al. (2002). The formation of pseudobrookite records minimum temperatures of about 585 ± 10 °C (Haggerty and Lindsley, 1970).

Silica activity was determined with QUILF in the rock types of the main intrusive phase from the above-mentioned assemblage of Fe–Mg silicate minerals and Fe–Ti oxides. The calculated values are relatively low ranging from 0.5 to 0.6 in the phonolite and from 0.4 to 0.5 in both nepheline syenites. Unit activity of SiO_2 was referred to a standard state of a pure SiO_2 modification at P and T.

5.3. Oxygen fugacity

For phase I rocks, relative oxygen fugacity varies between 0.5 and 1.9 log units above the synthetic FMQ buffer indicating relatively oxidized conditions. For the late-magmatic stage at the Katzenbuckel, the only constraint on oxygen fugacity is the secondary pseudobrookite–hematite assemblage of the metasomatically altered phonolite (KbU2) indicating a high-temperature oxidation. Additionally, hematite occurs in some alkali feldspar syenite dykes. This indicates conditions of formation above the synthetic HM buffer and an increase of the oxygen fugacity in phase II (Fig. 10).

6. Discussion

6.1. Evolution of oxygen fugacity during fractionation

The petrological investigations have the following implications for the fractionation of the Katzenbuckel melts. Already the least fractionated rocks of phase I indicate relatively oxidized conditions above the FMQ buffer. During cooling, the assemblage of olivine, clinopyroxene, ilmenite and magnetite buffers oxygen fugacity and the melt develops parallel to the FMQ buffer. In the late-magmatic stage, an increase in oxygen fugacity culminates in the formation of hematite and in some places pseudobrookite at still relatively high temperatures and conditions above the HM buffer (short bold arrow in Fig. 10). Moreover, in most rock types arfvedsonite and aegirine occur as late-magmatic minerals, which also indicates a relative increase in oxygen fugacity (e.g., Marks et al., 2003).

Similar evolution trends are known from other peralkaline rock suites and quantitative data on crystallization parameters are available from two examples of the Gardar province, South Greenland (Ilímaussaq, Markl et al. (2001); Puklen, Marks et al. (2003)). The early Ilímaussaq augite syenite shows an internal development towards more reducing conditions with values between 2 and 4 log units below FMQ, thus representing the most reduced conditions known from alkaline complexes so far. With the formation of highly fractionated agpaitic rocks, oxygen fugacity rises. The increase in oxygen

Table 6
Representative electron microprobe analyses of biotites and amphiboles from the Katzenbuckel

Mineral	Bio	Bio	Bio	Bio	Bio	Magnesio-katophorite	Magnesio-katophorite	Richterite	Ferric-nyböite	Ferric-nyböite	Magnesio-arfvedsonite
Sample	Kb22	Kb25	Kb25	Kb31	Kb47dyke1	Kb22	Kb24	Kb49	Kb25	KbU6	Kb50
Rock type	Nepheline syenite	Nepheline syenite	Nepheline syenite	Tinguaite	Alkali feldspar syenite dyke	Nepheline syenite	Nepheline syenite	Alkfsp syenite dyke with magnetite veins	Nepheline syenite	Tinguaite	Metasom. altered alkali feldspar syenite dyke
wt.%											
SiO_2	40.06	35.07	38.58	39.18	41.04	50.89	50.73	53.22	48.53	50.94	53.05
TiO_2	8.57	12.78	9.03	5.34	4.71	4.87	3.68	4.22	5.71	3.97	2.65
Al_2O_3	9.76	13.13	10.62	8.52	10.77	2.58	3.09	1.01	1.86	1.85	1.83
BaO	0.00	2.65	0.37	0.00	0.00	–	–	–	–	–	–
Fe_2O_3 (calc.)*						0.00	0.00	0.00	3.50	4.55	6.59
FeO	10.88	11.77	12.56	20.80	6.27	8.19	9.03	12.77	15.32	12.01	5.88
MnO	0.19	0.13	0.23	0.72	0.32	0.29	0.18	1.48	0.62	0.49	0.35
MgO	16.60	11.94	14.63	12.11	21.43	16.27	16.06	12.90	9.47	12.05	15.36
CaO	0.01	0.02	0.03	0.02	0.02	6.08	4.38	2.68	1.37	2.18	0.80
Na_2O	0.72	0.73	0.66	0.50	0.68	6.09	6.88	8.02	7.77	7.95	9.57
K_2O	9.41	7.80	8.90	9.37	9.73	1.89	1.75	1.05	2.79	2.35	1.15
ZrO_2	–	–	–	–	–	0.11	1.28	0.07	0.32	0.12	0.15
Cl	0.01	0.08	0.01	0.02	0.01	0.01	0.01	0.01	0.00	0.01	0.00
F	2.43	0.22	0.43	1.33	1.89	1.76	2.45	0.26	0.44	0.91	2.41
Total	98.64	96.32	96.05	97.91	96.87	99.03	99.52	97.69	97.70	99.38	99.79
	Formulae based on 22 oxygens					Formulae based on 16 cations and 23 oxygens					
Si	5.84	5.25	5.72	5.99	5.92	7.42	7.40	7.85	7.37	7.49	7.63
Al	1.68	2.31	1.85	1.53	1.83	0.44	0.53	0.18	0.33	0.32	0.31
Ti	0.94	1.44	1.01	0.61	0.51	0.53	0.40	0.47	0.65	0.45	0.29
Zr	–	–	–	–	–	0.01	0.09	0.00	0.02	0.01	0.01
Fe^{3+}						0.00	0.00	0.00	0.40	0.50	0.71
Mg	3.61	2.66	3.23	2.76	4.61	3.54	3.49	2.84	2.15	2.64	3.29
Fe^{2+}	1.33	1.47	1.56	2.66	0.76	1.00	1.10	1.57	1.95	1.48	0.71
Mn	0.02	0.02	0.03	0.09	0.04	0.04	0.02	0.18	0.08	0.06	0.04
Ca	0.00	0.00	0.00	0.00	0.00	0.95	0.69	0.42	0.22	0.34	0.12
Na	0.20	0.21	0.19	0.15	0.19	1.72	1.95	2.29	2.29	2.27	2.68
K	1.75	1.49	1.68	1.83	1.79	0.35	0.33	0.20	0.54	0.44	0.21
Ba	0.00	0.16	0.02	0.00	0.00	–	–	–	–	–	–
Cl	0.00	0.02	0.00	0.00	0.00	0.00	0.00	0.00	0.00	0.00	0.00
F	1.12	0.10	0.20	0.64	0.86	0.81	1.13	0.12	0.21	0.42	1.10
Sum	15.37	15.01	15.29	15.62	15.65	16.00	16.00	16.00	16.00	16.00	16.00

fugacity is controlled by equilibria among arfvedsonite, aenigmatite and aegirine developing parallel to an experimentally determined curve along which these phases coexist (Ernst, 1962; labeled "Aeg+Arf" in Fig. 10). A similar evolution trend was found in the Puklen syenites. Initially, oxygen fugacity is well below the FMQ buffer and the late-stage formation of aegirine and hematite at the expense of arfvedsonite finally indicates an increase in oxygen fugacity above the HM buffer, though at much lower temperatures compared to Ilímaussaq and the Katzenbuckel (Fig. 10).

Obviously, oxygen fugacity in alkaline to peralkaline melts is buffered by several solid phase equilibria during most of their evolution. Among these, Ilímaussaq shows the most reducing starting conditions while in the melts of the Katzenbuckel, oxygen fugacity was relatively high. Although the initial redox state in such melts can be highly variable (the discussed melts reflect differences in oxygen fugacity of more than 4 log units) they all end up very similar at highly oxidized conditions with arfvedsonite–aenigmatite–aegirine–hematite assemblages at or above the HM buffer.

6.2. Influence of oxygen fugacity on major element mineral chemistry

Compared to other basic Rhinegraben volcanics, the Katzenbuckel rocks show low Ni (<30 ppm), Cr (<5

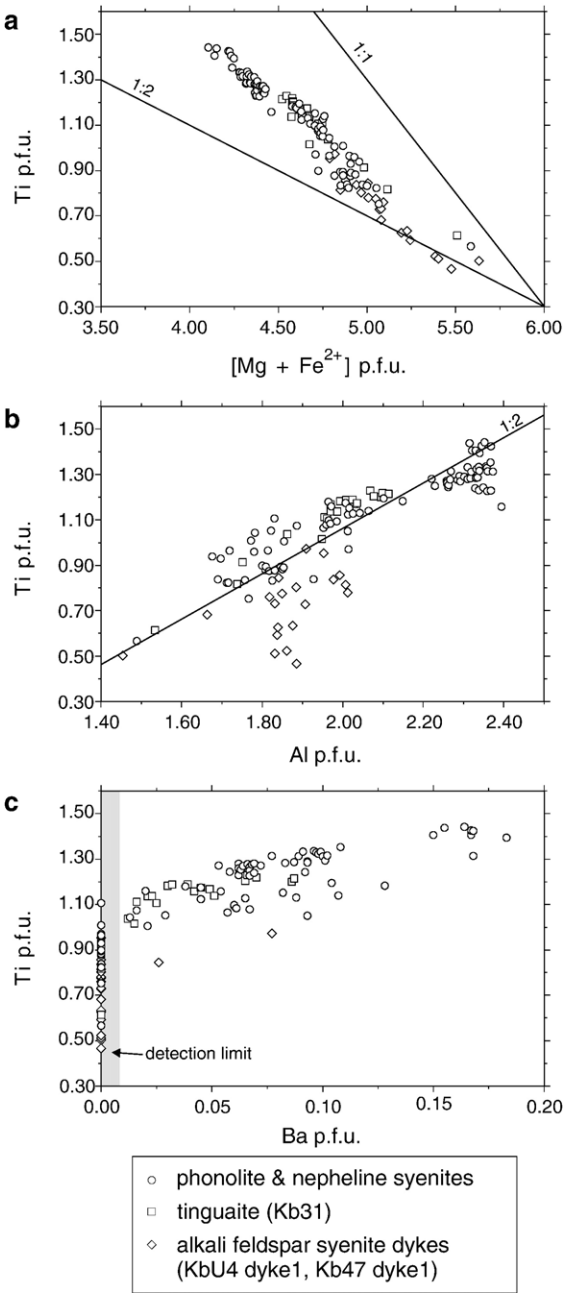

Fig. 8. Correlation diagrams for the Katzenbuckel biotites. (a) A strongly negative correlation between Ti and the two dominating elements on the octahedron position [Mg+Fe^{2+}] indicate an exchange of these elements. (b) A positive correlation between Ti and Al with a proportion of about 1 : 2 possibly indicates the coupled substitution of Mg^{2+}+2 Si<–>Ti^{4+}+2 Al. (c) The positive correlation between Ba and Ti in the Katzenbuckel suite, which is quite common in phlogopites from alkaline rocks.

ppm) and MgO (~5 wt.%) contents (Gehnes and Wimmenauer, 1975; Frenzel, 1975; Stähle et al., 2002) indicating considerable fractionation of the Katzenbuckel melts despite the relatively high Fo contents of olivines (up to 78 mol%). However, the relatively oxidized conditions found for the early magmatic stage led to a high Fe^{3+}/Fe^{2+} ratio in the Katzenbuckel melts, which in turn caused a relatively increased Mg^{2+}/Fe^{2+} ratio compared to melts with the same Mg/Fe_{tot} ratio at lower oxygen fugacities. This high Fe^{3+}/Fe^{2+} ratio was responsible for the crystallization of Mg-rich olivine and for the same reason, the other mafic phases (early clinopyroxene, amphibole, biotite) have high X_{Mg} values, which do not reflect a primitive melt composition but record the low Fe^{2+}/Fe^{3+} ratio in the melt caused by the high oxygen fugacity.

Most obviously, the oxidation state of such alkaline to peralkaline melts is reflected in their clinopyroxene compositional trends (Fig. 6a). Generally, pyroxene trends from alkaline suites evolve from diopsidic to Aeg-rich compositions (e.g. Woolley and Platt, 1988). However, the extent of the Fe^{2+}-enrichment in the course of their evolution varies significantly among different sample suites mainly depending on the oxidation state of the magma (e.g. Larsen, 1976). In that sense, the Katzenbuckel and the Ilímaussaq suite represent extremes at either end of the existing range. The highly reduced Ilímaussaq melts crystallized pyroxenes with the strongest enrichment in Fe^{2+} prior to evolution to Aeg-rich composition, whereas at the oxidized Katzenbuckel pyroxenes are extremely Fe^{2+}-poor (Fig. 6a). Thus, variation in clinopyroxene chemistry (in terms of their Fe^{2+}/Fe^{3+} ratio) appears to be a sensitive monitor of oxygen fugacity. Similar Fe^{2+}-poor clinopyroxene trends were reported from potassic rocks of Murun, Siberia (Fig. 10a, no. 1; Mitchell and Vladykin, 1996) and from Gordon Butte, Montana (Chakhmouradian and Mitchell, 2002; not shown on Fig. 6). Unfortunately, a determination of oxygen fugacities in these rocks was not possible. However, the partitioning of Fe^{2+} between clinopyroxene and co-existing mafic minerals was also shown to be of certain importance for the evolutionary trend of clinopyroxenes (Chakhmouradian and Mitchell, 2002; Piilonen et al., 1998).

Not only the pyroxenes record the high oxygen fugacity of the Katzenbuckel melts. The Fe^{3+} content of the melt must have been so high that even the felsic minerals incorporated Fe^{3+} in their structure. In both alkali feldspar and nepheline, Fe^{3+} contents reach exceptionally high values in the metasomatically altered phonolite (KbU2) where highly oxidizing conditions are recorded by the occurrence of hematite and pseudobrookite (see above).

The high oxidation state of the Katzenbuckel melts reflected by the major element composition

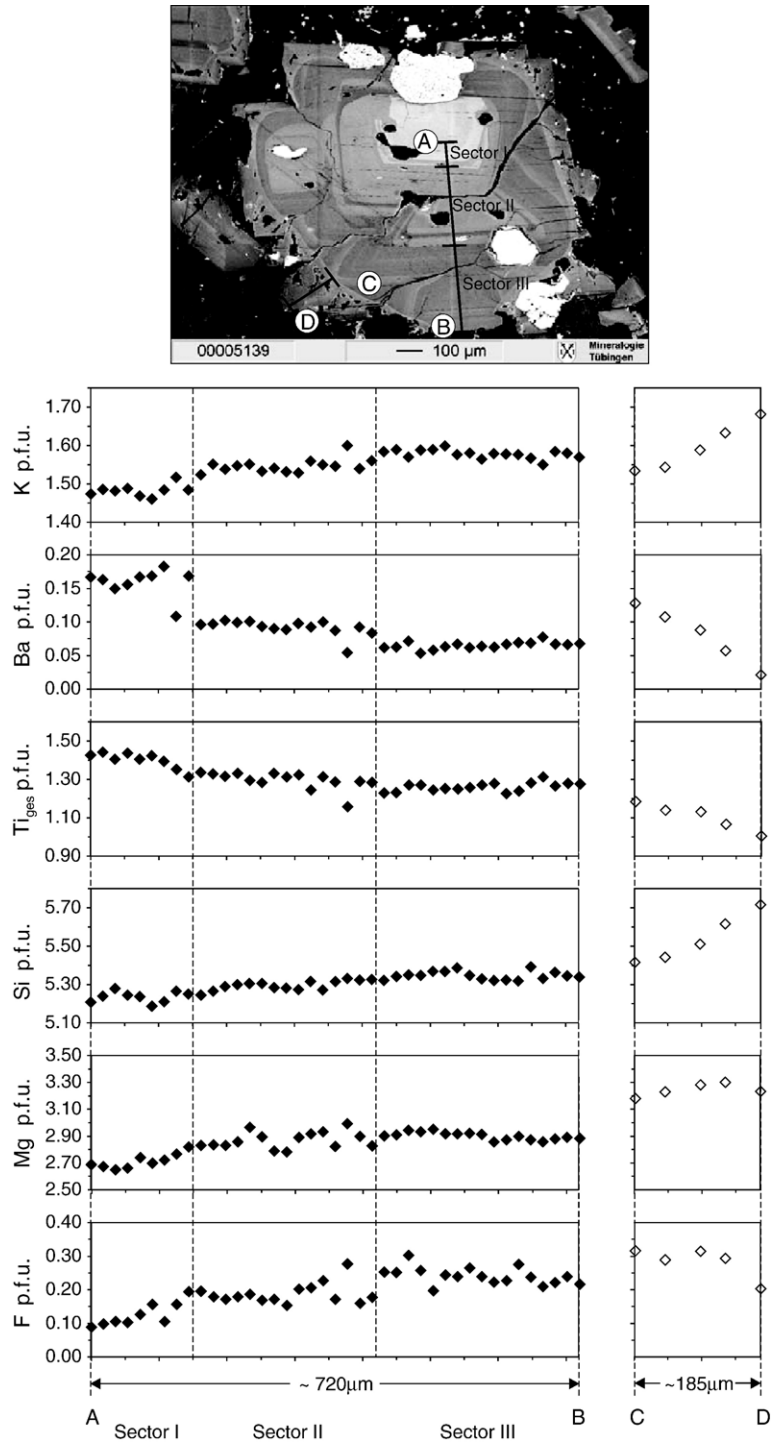

Fig. 9. Zoning profiles for a euhedral sector-zoned biotite of the nepheline syenite Kb25.

of the important rock-forming minerals is taken as evidence of a highly oxidized source region for the Katzenbuckel melts. Although the oxidation state of the Katzenbuckel even increases in the late-magmatic stage, the general oxidized character appears to be a source characteristic and is not believed to be induced by the interaction with meteoric fluids.

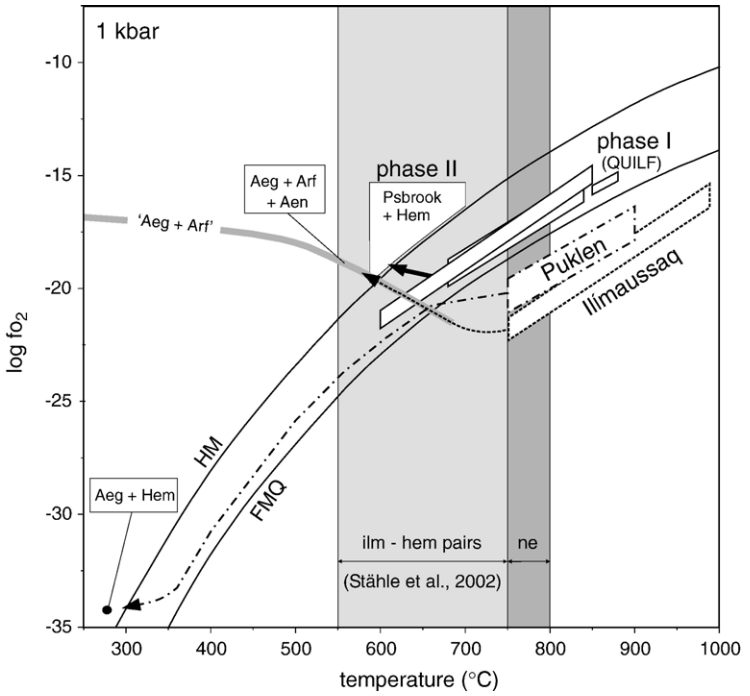

Fig. 10. $T-f_{O2}$ diagram showing calculated crystallization conditions for the Katzenbuckel rocks. Data for the alkaline complexes of Puklen and Ilímaussaq are from Markl et al. (2001) and Marks et al. (2003), respectively, and are shown for comparison.

6.3. Significance of minor element mineral chemistry

A typical feature of the Katzenbuckel melts is their strong enrichment in incompatible trace elements like Ba, Sr, Nb and especially Ti and Zr, which is reflected not only by the occurrence of rare late-magmatic accessory minerals but also by unusual compositions of the major rock-forming minerals. The most prominent example is again displayed by the pyroxenes, which are exceptionally rich in both Ti and Zr. Although Ti- and Zr-rich aegirines are well known from alkaline to peralkaline igneous rocks (e.g., Larsen, 1976; Shearer and Larsen, 1994; Jones and Peckett, 1980; Nielsen, 1979) similarly high concentrations of both Ti and Zr have so far only been reported by Duggan (1988). Among others, the most important factors used to explain Ti- and Zr-rich aegirine are melt composition and the absence of other Ti/Zr-bearing mineral phases and oxygen fugacity.

Experimental work (e.g., Watson, 1979; Watson and Harrison, 1983) showed, that the solubility of Zr in felsic liquids is critically dependent upon peralkalinity. Furthermore, solubility of Zr and Ti increases with F content in the silicate melt (Keppler, 1993). Thus, the high peralkalinity of the Katzenbuckel rocks (see Stähle et al., 2002) is an explanation for the high concentrations of Ti and Zr in the Katzenbuckel melts. Although theoretically, zircon saturation in phase I rocks was achieved based on whole-rock data (Gehnes and Wimmenauer, 1975; Stähle et al., 2002), no zircon crystallized. Possibly silica activity was too low for zircon to crystallize (see calculations above). The absence of Zr-minerals like eudialyte or baddeleyite at high Zr concentrations in the melts easily explains the high Zr contents of pyroxenes. However, aegirines of the zircon-bearing phase II rocks are not poorer in Zr than other Katzenbuckel rocks.

Many authors consider low oxygen fugacity in the melt as being responsible for high Ti and Zr contents in aegirine structure (e.g. Jones and Peckett, 1980; Larsen, 1976). According to the schematic equilibrium $Fe^{2+}+Ti/Zr=2\ Fe^{3+}$, a high Fe^{2+}/Fe^{3+} ratio in the melt should favor high Ti and Zr contents in aegirine. Thus, the oxidized Katzenbuckel melts should crystallize rather Ti- and Zr-poor aegirine. However, for the relatively Fe^{2+} poor, but Mg-rich Katzenbuckel rocks, the above mentioned equilibrium does not hold, but can be written as $Mg^{2+}+Ti/Zr=2\ Fe^{3+}$. Thus, in the case of the Katzenbuckel, it is not oxygen fugacity but possibly the relatively high initial concentrations of Ti and Zr in the melt that are

responsible for the high Ti and Zr concentrations in aegirines. High Ti contents in the melts are also recorded by the magnetite compositions that show Usp components up to 55 mol% despite the highly oxidizing conditions and by high Ti contents in amphibole and biotite. The considerable amounts of Ti in the major mineral phases of the Katzenbuckel rocks do not only reflect the strong enrichment of this trace element during fractionation but point towards a Ti-rich source for the melts.

6.4. Constraints on possible source regions for the Katzenbuckel melts

The present investigation of the mineral chemistry and petrology of the Katzenbuckel suite confirms its exceptional position within the European volcanic province. Their high relative oxygen fugacity and their highly peralkaline character point to an unusual composition of the melt source. All observations reported above are best explained, if they are interpreted as primary features of the source as they are already documented within the least fractionated rocks of phase I. Thus, we assume a metasomatically enriched lithosphere as a major source for the Katzenbuckel melts, which was already proposed by Wilson and Downes (1991, 1992) as an important source region for the Cenozoic alkaline magmatism in central Europe. However, primitive magmas from many localities are believed to include also contributions from the asthenosphere, ranging from direct (Goes et al., 1999; Haase et al., 2004) to indirect involvement of a mantle plume, with the latter causing a metasomatic overprint of the lower lithosphere (Wilson et al., 1995; Dunworth and Wilson, 1998; Haase et al., 2004). At other localities, an asthenospheric component may be present as a metasomatically enriched upper mantle region only, which may be the result of the preceding geological events, i.e. the recycling of oceanic lithosphere during the Variscan orogeny (Wilson and Downes, 1991, 1992). One reason for the unusual melt composition and source characteristics of the Katzenbuckel rocks might be that inhomogeneity of the lithosphere is a rather small-scale phenomenon that is intimately connected with the complex processes during the Variscan orogeny.

7. Summary

The present mineral chemical and petrological study of the Katzenbuckel rocks highlights their exceptional position within the European volcanic province as well as compared to other peralkaline igneous suites worldwide. The most interesting deviation from typical evolution trends of peralkaline igneous suites is the highly oxidized character (0.5 to 1.9 log units above the FMQ buffer) of the rocks during their early magmatic stage at temperatures between 780 and 880 °C. The highly oxidized conditions during the early evolution of the Katzenbuckel melts led to an early enrichment of Fe^{3+} in magmatic clinopyroxenes and to the formation of Fe^{3+}-rich alkali feldspar and nepheline. During their late magmatic evolution, a further increase in oxygen fugacity resulted in redox conditions well above the HM buffer, which is typical for the late-stage evolution of peralkaline melts.

Typical for peralkaline rocks in principal, but exceptional for the European volcanic province, the Katzenbuckel rocks are highly enriched in trace elements like Ti, Zr, Nb, Ba, Sr, P and others. This results in unusual compositions of the rock-forming minerals as well as the accessory phases. For example, clinopyroxenes show exceptionally high concentrations of TiO_2 (8.5 wt.%) and ZrO_2 (6.2 wt.%), respectively. Besides high amounts of the Ti-aegirine endmember, a here newly defined Ca-(Ti, Zr)-clinopyroxene component with a chemical formula of Ca-(Ti, Zr)$_{0.5}$(Mg, Fe^{2+})$_{0.5}AlSiO_6$ contributes significantly to the composition of the Katzenbuckel clinopyroxenes. The enrichment of the above-mentioned elements, not only in pyroxene, but also in amphibole, biotite, Fe–Ti oxides and apatite and in the various accessory minerals point to a metasomatically enriched lithosphere as a possible source for these melts. Compared to the European volcanic province as a whole, the exceptional melt composition and source characteristics of the Katzenbuckel rocks indicate that metasomatic enrichment processes in the lithosphere might be rather small-scale phenomena, which were intimately connected to complex tectonic processes during the Variscan orogeny.

Acknowledgements

T. Wenzel is thanked for his help during microprobe measurements and for his comments on an earlier version of this manuscript. We also thank V. Stähle for providing sample material and A. Chakhmouradian and an anonymous reviewer for constructive comments, which helped to improve the quality of this work.

Appendix A. Calculation of clinopyroxene endmembers in the eight component system Di–Hd–En–Fs–Ac–Jd–Ti-Aeg–Ca-(Ti, Zr)-comp

Endmember	Chemical formula	Calculation	Conditions/restrictions
Aegirine (Aeg)	$NaFe^{3+}Si_2O_6$	$=Fe^{3+}*100$	if $Fe^{3+} \leq Na$
		$=Na*100$	if $Fe^{3+} > Na$
Jadeite (Jd)	$NaAlSi_2O_6$		(if $Al_{okt>}$ 0 and $(Na-Ac)>0$)
		$=Al_{okt}*100$	if $Al_{okt} \leq (Na-Ac)$
		$=(Na-Ac)*100$	if $Al_{okt} > (Na-Ac)$
(Ti, Zr)-aegirine ((Ti, Zr)-Aeg)	$Na(Ti, Zr)_{0.5}(Fe^{2+}, Mg)_{0.5}Si_2O_6$		(if $(Na-Ac-Jd)>0$ and $(Ti+Zr)>0$)
		$=(Na-Ac-Jd)*100$	if $(Na-Ac-Jd) \leq 2*(Ti+Zr)$
		$=2*(Ti+Zr)*100$	if $(Na-Ac-Jd) > 2*(Ti+Zr)$
Ca-(Ti, Zr)-component (Ca-(Ti, Zr)-comp.)	$Ca-(Ti, Zr)_{0.5}(Fe^{2+}, Mg)_{0.5}AlSiO_6$		(if $(Ti+Zr)_{rest}]>0$ and $Al_{tetr}>0$)
		$=2*(Ti+Zr)_{rest}^{1}*100$	if $2*(Ti+Zr)_{rest} \leq Al_{tetr}$ and $2*(Ti+Zr)_{rest} \leq Ca$
		$=Al_{tetr}*100$	if $2*(Ti+Zr)_{rest} > Al_{tetr}$ and $Al_{tetr} \leq Ca$
		$=Ca*100$	if $Ca < 2*(Ti+Zr)_{rest}$ and $Ca < Al_{tetr}$
Diopside (Di)	$CaMgSi_2O_6$		(if $M^{2+}_{rest}>0$ and $Ca_{rest}>0$)
		$=Ca_{rest}^{2}*(1-X_{Fe}^{3})*100$	if $M^{2+}_{rest} \geq Ca_{rest}$
		$=M^{2+}_{rest}*(1-X_{Fe})*100$	if $M^{2+}_{rest} < Ca_{rest}$
Hedenbergite (Hd)	$CaFeSi_2O_6$		(if $M^{2+}_{rest}>0$ and $Ca_{rest}>0$)
		$=Ca_{rest}*X_{Fe}*100$	if $M^{2+}_{rest} \geq Ca_{rest}$
		$=M^{2+}_{rest}*X_{Fe}*100$	if $M^{2+}_{rest} < Ca_{rest}$
Enstatite (En)	$Mg_2Si_2O_6$		(if $M^{2+}_{rest}>0$ and $Ca_{rest}=0$)
		$=0.5*(M^{2+4}_{rest}-Ca_{rest})*(1-X_{Fe})*100$	if $M^{2+}_{rest} \geq Ca_{rest}$
Ferrosilite (Fs)	$Fe_2Si_2O_6$		(if $M^{2+}_{rest}>0$ and $Ca_{rest}=0$)
		$=0.5*(M^{2+}_{rest}-Ca_{rest})*X_{Fe}*100$	if $M^{2+}_{rest} \geq Ca_{rest}$

[1]: $(Ti+Zr)_{rest}=[(Ti+Zr)-(0.5*Ti\text{-}Aeg)]$, [2]: $Ca_{rest}=Ca-Ca\text{-}(Ti, Zr)\text{-comp.}$, [3]: $X_{Fe}=(Fe^{2+}+Mn)/(Mg+Fe^{2+}+Mn)$, [4]: $M^{2+}_{rest}=[(Mg+Fe^{2+}+Mn)-(0.5*Ti\text{-}Aeg)-(0.5*Ca\text{-}(Ti, Zr)\text{-comp.}$

References

Andersen, D.J., Lindsley, D.H., Davidson, P.M., 1993. QUILF: a PASCAL program to assess equilibria among Fe–Mg–Mn–Ti oxides, pyroxenes, olivine, and quartz. Comput. Geosci. 19, 1333–1350.

Armstrong, J.T., 1991. Quantitative elemental analysis of individual microparticles with electron beam instruments. In: Heinrich, K.F.J., Newbury, D.E. (Eds.), Electron Probe Quantitation. Plenum Press, New York, pp. 261–315.

Bowles, J.F.W., 1988. Definition and range of composition of naturally occurring minerals with the pseudobrookite structure. Am. Mineral. 73, 1377–1383.

Buddington, A.F., Lindsley, D.H., 1964. Iron–titanium oxide minerals and synthetic equivalents. J. Petrol. 5, 310–357.

Chakhmouradian, A.R., Mitchell, R.H., 2002. The mineralogy of Ba- and Zr-rich alkaline pegmatites from Gordon Butte, Crazy Mountains, Montana, (USA): comparisons between potassic and sodic agpaitic pegmatites. Contrib. Mineral. Petrol. 143, 93–114.

Coulson, I.M., 2003. Evolution of the North Qôroq centre nepheline syenites, South Greenland: alkali-mafic silicates and the role of metasomatism. Mineral. Mag. 67, 873–892.

Deer, W.A., Howie, R.A., Zussman, J., 1963. The Rock Forming Minerals, vol. 4, Framework Silicates. Longman, England.

Deer, W.A., Howie, R.A., Zussman, J., 1992. An Introduction to the Rock Forming Minerals, 2nd edition. Longman, England. 696 pp.

Della Ventura, G., Robert, J.-L., Beny, J.-M., 1991. Tetrahedrally coordinated Ti^{4+} in synthetic Ti-rich potassic richterites: evidence from XDR, FTIR and Raman study. Am. Mineral. 76, 1134–1140.

Duggan, M.B., 1988. Zirconium-rich sodic pyroxenes in felsic volcanics from the Warrumbungle Volcano, Central New South Wales, Australia. Mineral. Mag. 52, 491–496.

Dunworth, E.A., Wilson, M., 1998. Olivine melilitites of the SW German Tertiary volcanic province; mineralogy and petrogenesis. J. Petrol. 39, 1805–1836.

Edgar, A.D., Parker, L.M., 1974. Comparison of melting relationships of some plutonic and volcanic peralkaline undersaturated rocks. Lithos 7, 263–273.

Ernst, W.G., 1962. Synthesis, stability relations, and occurrences of riebeckite and riebeckite–arfvedsonite solid solutions. J. Geol. 70, 689–736.

Ferguson, A.K., 1977. The natural occurrence of aegirine–neptunite solid solution. Contrib. Mineral. Petrol. 60, 247–253.

Frenzel, G., 1953. Die Erzparagenese des Katzenbuckels im Odenwald. Beitr. Mineral. Petrol. 3, 409–444.

Frenzel, G., 1955. Die Eisenerzmineralien in natuerlich erhitzten Vulkaniten. Fortschr. Mineral. 33, 142–143.

Frenzel, G., 1961. Ein neues Mineral: Freudenbergit $Na_2Fe_2Ti_7O_{18}$. N. Jb. Mineral. Monatshefte, 12–22.

Frenzel, G., 1967. On petrochemistry and genesis of the volcanic rocks from the Katzenbuckel, Odenwald). The Rhinegraben progress report 1967. Bad. Geol. Landesamt, Abh.; Alsace-Lorraine, Serv. Carte Geol., Mem. vol. 6, pp. 131–134.

Frenzel, G., 1975. Die Nephelingesteinsparagenese des Katzenbuckels im Odenwald. Aufschluβ. Sonderband 27, 213–228.

Freudenberg, W., 1906. Geologie und Petrographie des Katzenbuckels im Odenwald. Mitt. Bad. Geol. Landesanst. 5, 185–344.

Frost, B.R., Lindsley, D.H., 1992. Equilibria among Fe–Ti oxides, pyroxenes, olivine, and quartz: part II. Application. Am. Mineral. 77, 1004–1020.

Gehnes, P., Wimmenauer, W., 1975. Geochemical studies on igneous rocks of the Rhine graben region, (Germany). N. Jb. Mineral. 2, 49–56.

Goes, S., Spakman, W., Bijward, H., 1999. A lower mantle source for Central European volcanism. Science 286, 1928–1931.

Granet, M., Wilson, M., Achauer, U., 1995. Imaging a mantle plume beneath the French Massif Central. Earth Planet. Sci. Lett. 136, 281–296.

Grapes, R., Yagi, K., Okumura, K., 1979. Aenigmatite, sodic pyroxene, arfvedsonite and associated minerals in syenites from Morotu, Sakhalin. Contrib. Mineral. Petrol. 69, 97–103.

Haase, K.M., Goldschmidt, B., Garbe-Schönberg, C.-D., 2004. Petrogenesis of tertiary continental intra-plate lavas from westerwald region, Germany. J. Petrol. 45, 883–905.

Haggerty, S.E., Lindsley, D.H., 1970. Stability of the pseudobrookite (Fe_2TiO_5)-ferropseudobrookite ($FeTi_2O_5$) series. Carn. Inst. Wash. Year Book, pp. 247–249.

Hamilton, D.L., 1961. Nephelines as crystallisation temperature indicators. J. Geol. 69, 321–329.

Hogarth, D.D., Chao, G.Y., Townsend, M.G., 1987. Potassium- and fluorine-rich amphiboles from the Gatineau area, Quebec. Can. Mineral. 25, 739–753.

Jones, A.P., Peckett, A., 1980. Zirconium-bearing aegirines from Motzfeldt, South Greenland. Contrib. Mineral. Petrol. 75, 251–255.

Keppler, H., 1993. Influence of fluorine on the enrichment of high field strength trace elements in granitic rocks. Contrib. Mineral. Petrol. 111, 113–121.

Khomyakov, A.P. 1995. Mineralogy of Hyperagpaitic Alkaline Rocks. Oxford Scientific Publications, Clarendon Press, Oxford. 222 pp.

Kogarko, L.N., Romanchev, B.P., 1977. Temperature, pressure, redox conditions, and mineral equilibria in agpaitic nepheline syenites and apatite–nepheline rocks. Geochem. Int. 14, 113–128.

Korobeinikov, A.N., Laajoki, K., 1994. Petrological aspects of the evolution of clinopyroxene composition in the intrusive rocks of the Lovozero alkaline massif. Geochem. Int. 31, 69–76.

Kretz, R., 1983. Symbols for rock-forming minerals. Am. Mineral. 68, 277–279.

Larsen, L.M., 1976. Clinopyroxenes and coexisting mafic minerals from the alkaline Ilímaussaq intrusion, South Greenland. J. Petrol. 17, 258–290.

Larsen, L.M., Sørensen, H., 1987. The Ilímaussaq intrusion-progressive crystallization and formation of layering in an agpaitic magma. In: Fitton, J.G., Upton, B.G.J. (Eds.), Alkaline Igneous Rocks, Geol. Soc. Sp. Publ. vol. 30, pp. 473–488.

Lattermann, G., 1887. Neue Untersuchungen an den Nephelingesteinen des Katzenbuckels im Odenwald. Unpubl. PdD thesis, Universität Heidelberg.

Le Maitre, R.W. (Ed.), 2002. Igneous Rocks; A Classification and Glossary of Terms; Recommendations of the International Union of Geological Sciences Subcommission on the Systematics of Igneous Rocks. Cambridge University Press, Cambridge. 236 pp.

Leake, B.E., Wooley, A.R., Arps, C.E.S., Birch, W.D., Gilbert, M.C., Grice, J.D., Hawthorne, F.C., Kato, A., Kisch, H.J., Krivovichev, V.G., Linthout, K., Laird, J., Mandarino, J.A., Maresch, W.V., Nickel, E.H., Rock, N.M.S., Schumacher, J.C., Smith, D.C., Stephenson, N.C.N., Ungaretti, L., Whittaker, E.J.W., Youzhi, G., 1997. Nomenclature of amphiboles: report of the Subcommittee on Amphiboles of the International Mineralogical Association, Commission on New Minerals and Mineral Names. Am. Mineral. 82, 1019–1037.

Lindsley, D.H., Frost, B.R., 1992. Equilibria among Fe–Ti oxides, pyroxenes, olivine, and quartz: Part I. Theory. Am. Mineral. 77, 987–1003.

Lippolt, H.J., Genter, W., Wimmenauer, W., 1963. Altersbestimmungen nach der Kalium-Argon-Methode an tertiären Eruptivgesteinen Südwestdeutschlands. Jb. Geol. Landesamt Baden-Württemberg 6, 507–538.

Lippolt, H.J., Horn, P., Todt, W., 1976. Kalium-Argon-Altersbestimmungen an tertiären Vulkaniten des Oberrheingraben-Gebiets; IV, Kalium-Argon-Alter von Mineralen und Einschlüssen der Basalt-Vorkommen Katzenbuckel und Rossberg. N. Jb. Mineral. Abh. 127, 242–260.

Markl, G., 1998. The Eidsfjord anorthosite, Vesterhålen, Norway: field observations and geochemical data. Norges Geol. Unders. Bull. 434, 53–75.

Markl, G., Baumgartner, L., 2002. pH changes in peralkaline late magmatic fluids. Contrib. Mineral. Petrol. 144, 331–346.

Markl, G., Marks, M., Schwinn, G., Sommer, H., 2001. Phase equilibrium constraints on intensive crystallization parameters of the Ilímaussaq Complex, South Greenland. J. Petrol. 42, 2231–2258.

Marks, M., Markl, G., 2001. Fractionation and assimilation processes in the alkaline augite syenite unit of the Ilímaussaq Intrusion, South Greenland, as deduced from phase equilibria. J. Petrol. 42, 1947–1969.

Marks, M., Vennemann, T., Siebel, W., Markl, G., 2003. Quantification of magmatic and hydrothermal processes in a peralkaline syenite–alkali granite complex based on textures, phase equilibria, stable and radiogenic isotopes. J. Petrol. 44, 1247–1280.

Mitchell, R.H., Vladykin, N.V., 1996. Compositional variation of pyroxene and mica from the little murun ultrapotassic complex, Aldan Shield, Russia. Mineral. Mag. 60, 907–925.

Morogan, V., 1989. Mass transfer and REE mobility during fenitization at Alnö, Sweden. Contrib. Mineral. Petrol. 103, 25–34.

Nielsen, T.F.D., 1979. The occurence and formation of Ti-aegirines in peralkaline syenites; an example from the Tertiary ultramafic alkaline Gardiner complex, East Greenland. Contrib. Mineral. Petrol. 69, 235–244.

Njonfang, E., Nono, A., 2003. Clinopyroxene from some felsic alkaline rocks of the Cameroon Line, Central Africa: Petrological implications. Eur. J. Mineral. 15, 527–542.

Oberti, R., Ungaretti, L., Cannillo, E., Hawthorne, F.C., 1992. The behaviour of Ti in amphiboles: I. Four-and six-coordinate Ti in richterite. Eur. J. Mineral. 4, 425–439.

Ottemann, J., Frenzel, G., 1965. Der Chemismus der Pseudobrookite von Vulkaniten, eine Untersuchung mit der Elektronen-Mikrosonde). Schweiz. Mineral. Petrogr. Mitt. 45, 819–836.

Piilonen, P.C., McDonald, A.M., Lalonde, A.E., 1998. The crystal chemistry of aegirine from Mont Saint-Hilaire, Quebec. Can. Mineral. 36, 779–791.

Potter, J., Rankin, A.H., Treloar, P.J., 2004. Abiogenic Fischer-Tropsch synthesis of hydrocarbons in alkaline igneous rocks; fluid inclusion, textural and isotopic evidence from the Lovozero complex, N.W. Russia. Lithos 75, 311–330.

Powell, M., 1978. The crystallisation history of the Igdlerfigssalik nepheline syenite intrusion, Greenland. Lithos 11, 99–120.

Ranløv, J., Dymek, R.F., 1991. Compositional zoning in hydrothermal aegirine from fenites in the Proterozoic Gardar Province, South Greenland. Eur. J. Mineral. 3, 837–853.

Ritter, J.R.R., Jordan, M., Christensen, U.R., Achauer, U., 2001. A mantle plume below the Eifel volcanic fields, Germany. Earth Planet. Sci. Lett. 186, 7–14.

Rosenbusch, H., 1869. Der Nephelinit vom Katzenbuckel. Unpubl. PhD thesis, Universität Freiburg.

Salvi, S., Williams-Jones, A.E., 1990. The role of hydrothermal processes in the granite-hosted Zr, Y, REE deposit at Strange Lake, Quebec/Labrador: evidence from fluid inclusions. Geochim. Cosmochim. Acta 54, 2403–2418.

Shearer, C.K., Larsen, L.M., 1994. Sector-zoned aegirine from the Ilímaussaq alkaline intrusion, South Greenland: implications for trace-element behavior in pyroxene. Am. Mineral. 79, 340–352.

Sobolev, S.V., Zeyen, H., Granet, M., Achauer, U., Bauer, C., Werling, F., Altherr, R., Fuchs, K., 1997. Upper mantle temperatures and lithosphere-asthenosphere system beneath the French Massif Central constrained by seismic, gravity, petrologic and thermal observations. Tectonophysics 275, 143–164.

Sood, M.K., Edgar, A.D., 1970. Melting relations of undersaturated alkaline rocks. Medd. Grønl. 181. 41 pp.

Sørensen, H., 1997. The agpaitic rocks — an overview. Mineral. Mag. 61, 485–498.

Stähle, V., Koch, M., 2003. Primary and secondary pseudobrookite minerals in volcanic rocks from the Katzenbuckel alkaline complex, southwestern Germany. Schweiz. Mineral. Petrogr. Mitt. 83, 145–158.

Stähle, V., Koch, M., McCammon, C.A., Mann, U., Markel, G., 2002. Occurrence of low-Ti and high-Ti freudenbergite in alkali syenite dikes from the Katzenbuckel volcano, SW Germany. Can. Mineral. 40, 1609–1627.

Stephenson, D., 1972. Alkali clinopyroxenes from nepheline syenites of the South Qôroq Centre, south Greenland. Lithos 5, 187–201.

Taylor, R.C., King, B.C., 1967. The pyroxenes of the alkaline igneous complexes of Eastern Uganda. Mineral. Mag. 280, 5–22.

Wagner, C., Velde, D., Mokhtari, A., 1987. Sector-zoned phlogopites in igneous rocks. Contrib. Mineral. Petrol. 96, 186–191.

Watson, E.B., 1979. Zircon saturation in felsic liquids: experimental results and applications to trace element geochemistry. Contrib. Mineral. Petrol. 70, 407–419.

Watson, E.B., Harrison, T.M., 1983. Zircon saturation revisited; temperature and composition effects in a variety of crustal magma types. Earth Planet. Sci. Lett. 64, 295–304.

Wedepohl, H., Baumann, A., 1999. Central European Cenozoic plume volcanism with OIB characteristics and indications of a lower mantle source. Contrib. Mineral. Petrol. 136, 225–239.

Wilson, M., 1989. Igneous Petrogenesis; a Global Tectonic Approach. Chapman and Hall, Wenheim. 465 pp.

Wilson, M., Downes, H., 1991. Tertiary–Quaternary extension-related alkaline magmatism in western and central Europe. J. Petrol. 32, 811–849.

Wilson, M., Downes, H., 1992. Mafic alkaline magmatism associated with the European Cenozoic rift system. Geodynamics of rifting; Volume I, Case history studies on rifts; Europe and Asia. Tectonophysics 208, 173–182.

Wilson, M., Patterson, R., 2001. Intraplate magmatism related to short-wavelength convective instabilities in the upper mantle; evidence from the Tertiary–Quaternary volcanic province of western and central Europe. Spec. Pap. - Geol. Soc. Am. 352, 37–58.

Wilson, M., Rosenbaum, J.M., Dunworth, E.A., 1995. Melilitites: partial melts of the thermal boundary layer? Contrib. Mineral. Petrol. 119, 181–196.

Woolley, A.R., Platt, R.G., 1988. The peralkaline nepheline syenites of the Junguni intrusion, Chilwa province, Malawi. Mineral. Mag. 52, 425–433.